University of Plymouth

PEARL **https://pearl.plymouth.ac.uk**

Faculty of Science and Engineering School of Geography, Earth and Environmental Sciences

2014-07-03

Transient fluvial incision as an indicator of active faulting and Plio-Quaternary uplift of the Moroccan High Atlas

Boulton, Sarah

http://hdl.handle.net/10026.1/3826

10.1016/j.tecto.2014.06.032
Tectonophysics
Elsevier

All content in PEARL is protected by copyright law. Author manuscripts are made available in accordance with publisher policies. Please cite only the published version using the details provided on the item record or document. In the absence of an open licence (e.g. Creative Commons), permissions for further reuse of content should be sought from the publisher or author.

NOTICE: this is the author's version of a work that was accepted for publication in Tectonphysics. Changes resulting from the publishing process, such as peer review, editing, corrections, structural formatting, and other quality control mechanisms may not be reflected in this document. Changes may have been made to this work since it was submitted for publication. A definitive version was subsequently published in Tectonophysics, 633, 16 – 33, http://dx.doi.org/10.1016/j.tecto.2014.06.032**.**

Transient fluvial incision as an indicator of active faulting and Plio-Quaternary uplift of the Moroccan High Atlas.

S. J. Boulton[1*], M. Stokes[1], A. E. Mather[1]

*[1] School of Geography, Earth and Environmental Sciences, Plymouth University, Devon, PL4 8AA, UK. *corresponding author: sarah.boulton@plymouth.ac.uk*

ABSTRACT

One of the challenges facing Earth Scientists is to determine the extent to which geomorphic features can be used to extract tectonic signals from landscapes. Here, we quantitatively analyse the long profiles of rivers that drain southwards across the South Atlas Fault (SAF), a thrust fault that forms the southern margin of the High Atlas Mountains in Morocco, to derive new data on the Late Cenozoic activity of this fault system. River long profiles were extracted for 32 major rivers flowing southwards into the Ouarzazate Basin. Of these, eleven exhibit concave-up river profiles with a mean concavity of 0.64 and normalized steepness indices in the range 47.5 – 219.0 $m^{0.9}$. By contrast, 21 rivers exhibit at least one knickpoint upstream of the thrust front. Knickpoint height varies from 100 – 1300 m, with calculated incision at the range bounding fault ranging from 80-900 m, despite the drainage areas upstream of the knickpoint ranging over several orders of magnitude. In map view, knickpoint locations generally plot along sub-parallel lines and there are no obvious relationships with lithological units for knickpoints exhibiting slope-break morphology. Channel reaches below slope-break knickpoints have higher mean concavities (0.76) than above the knickpoint indicative. This observation combined with a lithological or river-capture origin for the knickpoints having been ruled out suggests that an increase in uplift rate along a planar fault zone during the Plio-Quaternary caused the initiation of the transient response (i.e., knickpoint formation) to a change in base-level observed in the river profiles. This uplift event can be correlated to the convective removal of the lithospheric root to the Atlas Mountains resulting in the anomalously high topography at the present day.

Keywords: knickpoint, knickzone, intracontinental mountain belt, uplift, Morocco.

CITATION: Boulton, S.J., Stokes, M., Mather, A.E., 2014. Transient fluvial incision as an indicator of active faulting and Plio-Quaternary uplift of the Moroccan High Atlas. Tectonophysics, 633, 16 – 33.

INTRODUCTION

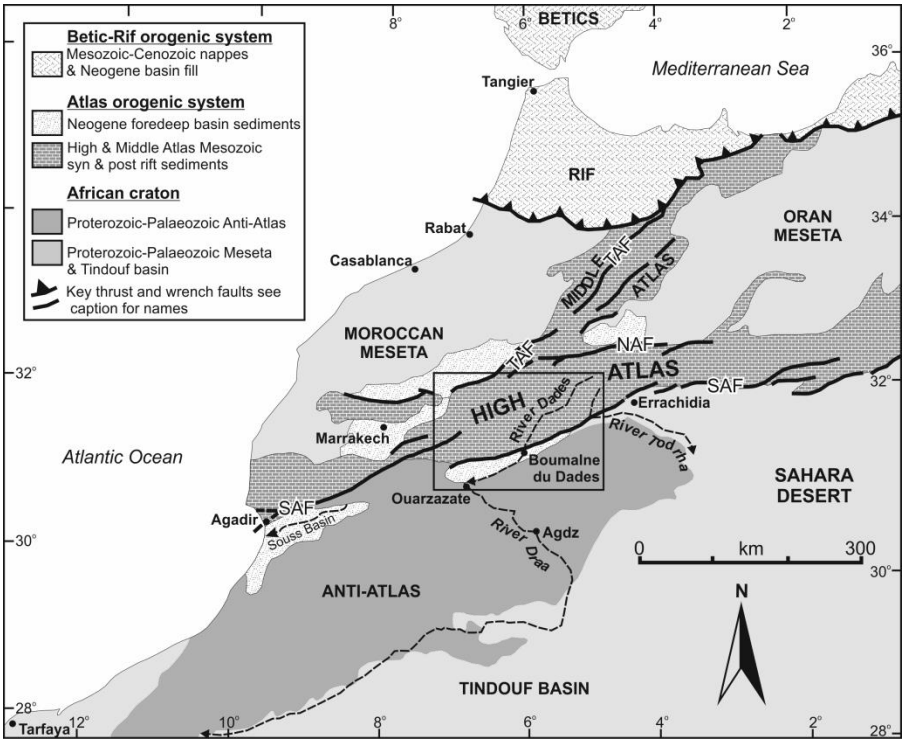

Figure 1. Overview map of Morocco showing the generalised geology of the Atlas orogenic system and associated major faults, with the Dades-Draa river system also shown (modified from Stokes et al., 2008). Box indicates areas shown in figures 2 and 3.

The High Atlas Mountains are a Cenozoic mountain belt trending ENE-WSW from Morocco in the west to Tunisia in the east (Fig. 1). Extending for over 2000 km, these mountains have the most significant relief in North Africa rising to over 4000 m in elevation. Alpine compression resulted in the inversion and uplift of Mesozoic rift basins between the Late Eocene and Quaternary (e.g., Frizon de Lamotte *et al*., 2000; Gomez *et al*., 2000; Teixell *et al*., 2003; Balestreri *et al*., 2009), developing a bivergent mountain chain with the South Atlas Fault (SAF) and the North Atlas Fault (NAF) as the southern and northern margins, respectively (Fig. 1). These two reverse faults accommodate a significant proportion of the shortening across the High Atlas, with the SAF generally having accommodated more Cenozoic shortening than the NAF (Sebrier *et al*., 2006). However, the Cenozoic tectonic shortening across the High Atlas only ranges from ~ 15 – 32% increasing eastwards along strike (Beauchamp *et al*., 1999; Teixell *et al*., 2003), insufficient to account for all of the high topography of this and surrounding areas. This anomalously high topography is considered to be isostatically uncompensated owing to the underlying lithosphere either being hot, thinned or delaminated, with perhaps as much as 1000 m of topography supported by underlying mantle processes (Seber *et al*., 1996; Ramdani, 1998; Teixell *et al*., 2003; 2005; Missenard *et al*., 2006; Miller *et al*., 2014). Furthermore, the partitioning of the growth of the High Atlas between recent (i.e., Quaternary) and pre-Miocene (> 25 Ma) uplift is poorly constrained. For example, Gomez *et al*., (2000) argues that all uplift has taken place since c. 20 Ma. This is

supported by thermochronology indicating that the present-day topographic relief was completely generated in the last 15 - 20 Ma (Barbero *et al*., 2007). Yet, this result is at odds with geological constraints on uplift that suggest that two pulses of surface uplift have occurred, one > 25 Ma and further uplift in the Plio-Quaternary (< 5 Ma), which correlate to the deposition of coarse-clastic material in the foreland(El Harfi *et al*., 2001; 2006). Additionally, Babault *et al*., (2008) and Balestrieri *et al*., (2009) suggest c. 1000 m of surface uplift has taken place during the Plio-Quaternary period based upon drainage reorganisation and fission-track analysis.

Current models of the development of the High Atlas are based primarily on geological methods. However, geomorphological approaches for examining tectonics and mountain belt development provide hitherto untried approaches for elucidating the styles, patterns and timing of High Atlas development. A major focus of current tectonic geomorphological research is to develop and apply methodologies to extract information about past and present tectonic activity from the landscape, principally by using river long profiles that have either reached a steady state (e.g., Whipple and Tucker, 1999; Synder et al., 2000; Wohl and Merritt, 2001; Kirby et al., 2003) or that exhibit a 'transient response' to a change in base level (e.g., Whipple and Tucker, 1999; 2002; Whipple, 2004; Whittaker et al., 2007; 2008; Boulton and Whittaker, 2009; Whittaker and Boulton, 2012). The river long profile plots channel elevation against distance downstream from the drainage divide and is sensitive not only to increases or decreases in tectonic uplift but also to variations in rock strength (Phillips and Lutz, 2008), river capture (Antón et al., 2012; 2014), sea-level controlled base-level change (Crosby and Whipple, 2006), climatic and other environmental landscape changes (Burbank and Anderson, 2001; Schumm, 2005).

Given the contradictions on the age and timing of uplift in the High Atlas, this study aims to elicit information on the recent uplift and activity of the region using the fluvial geomorphology of transverse drainages, since the recent 1 km of uplift should be recorded by a geomorphological landscape response. After outlining the regional geology, geomorphology and background to river profile analyses, we present geomorphic indices extracted from digital elevation models (DEMs) from 32 rivers draining the southern margin of the High Atlas Mountains. Competing controls on river profile geometry (lithology, river capture and uplift) are then compared and discussed in light of the results and implications for the tectonic activity of the central High Atlas and SAF drawn.

GEOLOGICAL BACKGROUND

South of the High Atlas, two foreland basins have developed during the Cenozoic as a result of lithospheric flexure in response to crustal loading (Beauchamp *et al*., 1999). These are the Souss Basin in the west and the Ouarzazate Basin in the east, separated by a topographic high of the Siroua Plateau (Fig. 1). The Ouarzazate Basin fill is < 1 km thick, composed of Mio-Pliocene alluvial, fluvial and lacustrine sediments (e.g., Saadi *et al*., 1978; Gorler *et al*., 1988; El Harfi *et al*., 2001; Teson *et al*., 2010). Palaeogeographic reconstructions of the Mio-Pliocene foreland basin fill reveal an internally drained lacustrine basin bordered by alluvial fans and transverse fluvial valleys that drained the dominant High and Anti-Atlas reliefs to the north and south (Gorler *et al*., 1988; El Harfi *et al*., 2001).

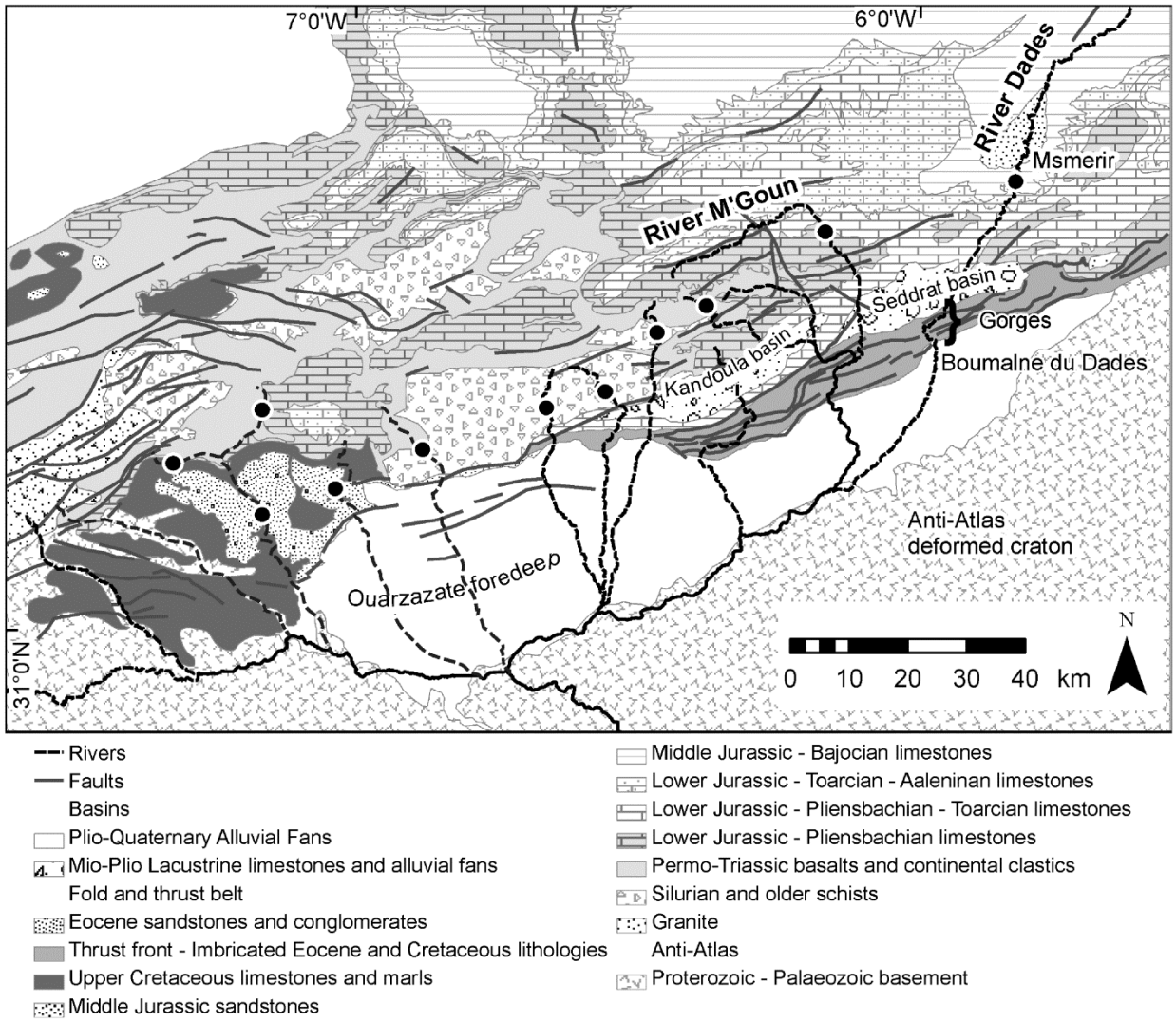

Figure 2. Simplified geological map of the Ouarzazate region showing the main geological units present, key locations, trunk rivers and (where present) knickpoints (modified from the Saadi et al., 1978).

Forming the northern margin of the Ouarzazate Basin, the SAF is a major structural feature that runs continuously along the length of the mountain chain. Structurally, the SAF is a complex fault zone composed of mainly thick-skinned deformation resulting from the inversion of Mesozoic normal faults, with minor thin-skinned deformation (Beauchamp *et al*., 1999; Teixell et al., 2003; El Harfi *et al*., 2006; Teson and Teixell, 2008). Continued faulting during the Miocene-Pleistocene resulted in foreland basin segmentation and the creation of a series of small wedge-top basins (Ait Kandoula in the west and Ait Sedratt in the east) to the north of the frontal thrust system (Fig. 2; Gorler *et al*., 1988; El Harfi *et al*., 2001; 2006; Teson and Teixell, 2008).

The SAF is considered to have accommodated most of the Cenozoic tectonic shortening across the High Atlas Mountains and is the focus of active deformation (Teixell *et al*., 2003; Sebrier *et al*., 2006; Pastor *et al*., 2012a). Although no direct estimates are available for the slip-rate along the thrust front in the Ouarzazate Basin, localised deformation of Quaternary terraces gives some

indication. Sebrier *et al*. (2006) document a faulted ramp anticline deforming their Q_3 alluvial fan surface. Although, this surface was not dated using absolute methods in their study, Sebrier *et al*. (2006) estimate a minimum shortening rate of 0.04 $mmyr^{-1}$ and a slip rate of 0.05-0.15 $mmyr^{-1}$ based upon a 12 m vertical offset and a maximum age of 5 Ma for the SAF. Subsequently, Arboleya *et al*. (2008) used ^{10}Be cosmogenic (TCN method) surface exposure dating to determine the chronology of a series of alluvial fan and river terrace surfaces, several of which they noted to be deformed. Their Q_2 terrace, with a calculated exposure age of 163-174 ka, was observed to be folded above a blind thrust causing a 20 m vertical offset of the terrace surface (Arboleya *et al*., 2008) equating to a minimum uplift rate of ~ 0.11 $mmyr^{-1}$. Whereas, higher uplift rates of 0.2 – 0.3 $mmyr^{-1}$ have been derived by Pastor *et al*. (2012a) from deformed terraces of the same age.

Active faulting is also supported by the distribution of generally shallow (< 70 km deep; Medina and Cherkaoui, 1991) earthquakes in the Atlas Mountains. Focal mechanisms indicate ~ NE-SW compressive to transpressive deformation along the edges of the range, although many earthquakes are also distributed within the mountains along other structural lineaments (Medina and Cherkaoui, 1991; Morel and Meghraoui, 1996; USGS, 2010; Onana *et al*., 2011). The most significant recorded earthquake along the thrust front was the 1960 Agadir earthquake (M = 5.9) situated near the Moroccan coast but Boumalne du Dades, in the study area, has also experienced earthquakes of M = 4.7 and 4.9 at or near the thrust front (Medina and Cherkaoui, 1991).

GEOMORPHOLOGIC BACKGROUND

The River Dades forms the principal drainage in the Ouarzazate basin. The headwaters of the river rise at ~3200 m and then drains SW (oblique to the trend of the orogeny), cutting a deeply incised ~225 km long route through the fold-thrust belt, wedge top basin, thrust front and foreland regions of the south-central part of the High Atlas orogenic system (Fig. 2). In the foreland basin, the Dades forms a transverse drainage fixed against the topographic relief of the northern margin of the Anti-Atlas Mountains (Stokes et al., 2008; Babault et al., 2012). Here, the Dades is joined by a series of major south-flowing transverse tributaries such as the Madri and the M'Goun (Fig. 3). In the southwest section of the foredeep, the Dades turns SE and crosses Pre-Cambrian and Palaeozoic bedrock of the Anti-Atlas Mountains through the Draa gorge (Fig. 1). To the east, rivers such as the Todrha drain into the Sahara Desert and to the west rivers drain into the Souss Basin (Fig. 1).

The Quaternary development of the River Dades and tributaries is recorded by a series of inset river terraces, alluvial fan surfaces and stepped fan pediments (Stablein, 1988; Arboleya *et al*. 2008; Pastor *et al*., 2012b), and in the formation of deeply dissected river gorges such as the Dades gorge (Stokes *et al*., 2008). The overall incisional pattern of the drainage network, including river gorge development, is considered to primarily reflect the long term tectonic uplift of the High Atlas orogenic system (Stablein, 1988; Stokes *et al*, 2008; Babault *et al*., 2012). Superimposed onto the uplift trend are sedimentation and erosion patterns, such as piedmont stream capture, linked to Quaternary climatic fluctuations (Arboleya *et al*., 2008; Pastor *et al*., 2012b). Evidence for cirques, troughs, moraines and other related features have been recorded in the Dades watershed area above 3 km altitude (Hughes *et al*., 2004) suggesting periodic glacial and periglacial activity within the south-central High Atlas region. This undoubtedly would have played some role in influencing variations in sediment supply and flood regime, which in turn would have impacted upon fluvial

landscape aggradation and dissection patterns downstream at lower altitudes. Finally, the incision history of the Dades could also reflect relative base-level adjustments to basin scale capture of the Dades by the Draa, resulting in a switch from an internally drained Mio-Pliocene foredeep basin to the externally drained modern drainage network (Gorler *et al*., 1988). The timing and nature of the capture mechanism have yet to be studied in detail, but cosmogenic exposure dating of the highest fan surface along the northern basin margin by Arboleya *et al*. (2008) suggests that basin incision commenced after 278 ka. The amount of post-capture incision is unclear. However, alluvial gravels preserved along the top edge of the Draa Gorge suggest < 200 m of incision (Arboleya *et al*., 2008) has occurred across the Proterozoic-Palaeozoic Anti-Atlas basement since the switch from internal to external drainage. The capture-related base-level lowering could be in part driving the incision observed in the immediately adjacent upstream foreland basin region.

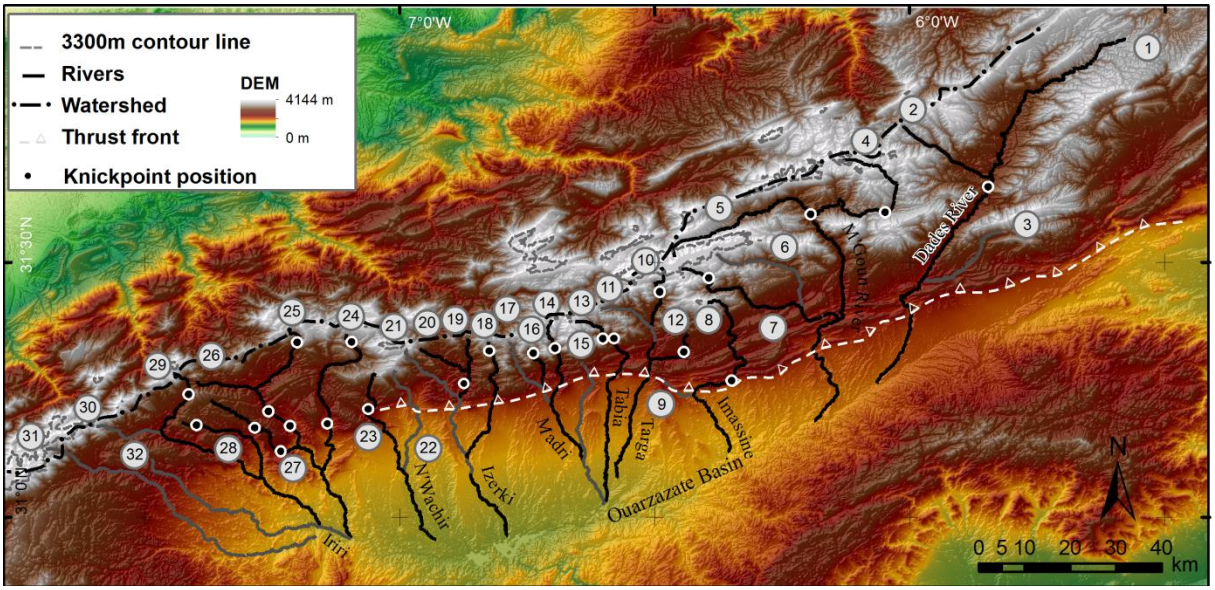

Figure 3. STRM DEM (USGS, 2006) of the area indicated in Figure 1, indicating the river long profiles extracted for this study. Each river is numbered corresponding to data in Table 1 and the long profile of selected rivers shown in figures 7, 8, 10.

RIVER PROFILE ANALYSIS

Steady-state profiles

Three broad models describing fluvial erosion have been developed: detachment-limited; transport-limited and hybrid models (e.g., Tucker and Whipple, 2002; Whipple and Tucker, 2002). In detachment-limited systems the steady-state (where erosion equals uplift) river gradient is controlled by the erodibility of the channel substrate and the regional uplift rate or base-level fall; these rivers are characteristically bedrock rivers. By contrast, the channel gradient in transport-limited systems is determined by the ability of the river to transport the sediment load, and such rivers are typically alluvial channels with a loose sediment cover in bars and banks. Hybrid rivers are intermediate cases between the end members of transport- and detachment-limited models, where the sediment flux and the ability to erode the bedrock substrate of the channel determines the channel gradient; both bedrock and alluvial reaches will be present along the course of the river.

These simple of models of river behaviour predict power law relationships between local channel gradients (*S*, slope) and upstream drainage area (*A*) in the form:

$$S = k_s A^{-\Theta} \quad (1)$$

Both *S* and *A* can be easily extracted from digital elevation models (DEMs) from the analysis of slope-area plots. Subsequently, the concavity index, Θ, and the steepness index, k_s, can be derived from the regression of slope and area data. As this general power-law function can be derived from the erosion law of all three river models (Whipple and Tucker, 2002; Kirby *et al*., 2003) the concave-up, presumed steady-state river long profile is identical for all types of river if the concavity and steepness are the same.

As eq [1] subsumes within k_s the uplift rate of a given area [k_s = (uplift/coefficient of erosion)$^{1/n}$] this term should vary systematically with uplift at steady state (Whipple and Tucker, 1999; 2002), a conclusion that has been supported by a range of empirical studies (i.e., Snyder *et al*., 2000; Kirby and Whipple, 2001; Safran *et al*., 2005; DiBiase *et al*., 2009; Cyr *et al*., 2010) and has been applied in many areas to examine both the suitability of erosion laws and to determine uplift rates (e.g., Tucker, 2009; Tucker and Hancock, 2010; Brocklehurst, 2010). Where there is no rock uplift, and in the absence of other confounding factors, the steepness index declines over time and may attain a low value set by the properties of the bedrock substrate (Whipple, 2004).

Rivers with transient features

Not all river long profiles exhibit a graded, concave-up profile with many having discontinuities in the channel profiles, which are identified on long profiles as convexities and on slope-area plots as breaks in the power-law scaling (e.g., Kirby and Whipple, 2012). In general the presence of knickpoints is indicative of a river undergoing a transient response to a perturbation where the knickpoint is not fixed on a particular feature but migrates upstream over time as a transient wave of incision (e.g., Harsbargen and Paola, 2000; Bishop *et al*., 2005; Wobus *et al*., 2006; Crosby and Whipple, 2008; Whittaker *et al*., 2008; Jansen *et al*., 2011; Castillo *et al*., 2013).

Knickpoints develop along rivers described by the detachment-limited and hybrid models as the result of one or more factors that may not be independent or mutually exclusive. These are: incision resulting from base-level lowering (either a local tectonic perturbation or regionally due to sea-level fall); variations in bedrock resistance; influence of bedrock structure; sediment input from hill slopes or tributaries; non-fluvial erosional processes such as debris flows; effects of bedload either as an erosive tool or mantling cover, river confluences, climatic fluctuations, or human modifications (Burbank and Anderson, 2001; Schumm, 2005; Phillips and Lutz, 2008). By contrast, transport-limited rivers generally respond in a diffusive manner to base-level fall and uplift and thus do not develop a knickpoint making it difficult to distinguish between steady-state and transient profiles in this category of river (Whipple and Tucker, 2002).

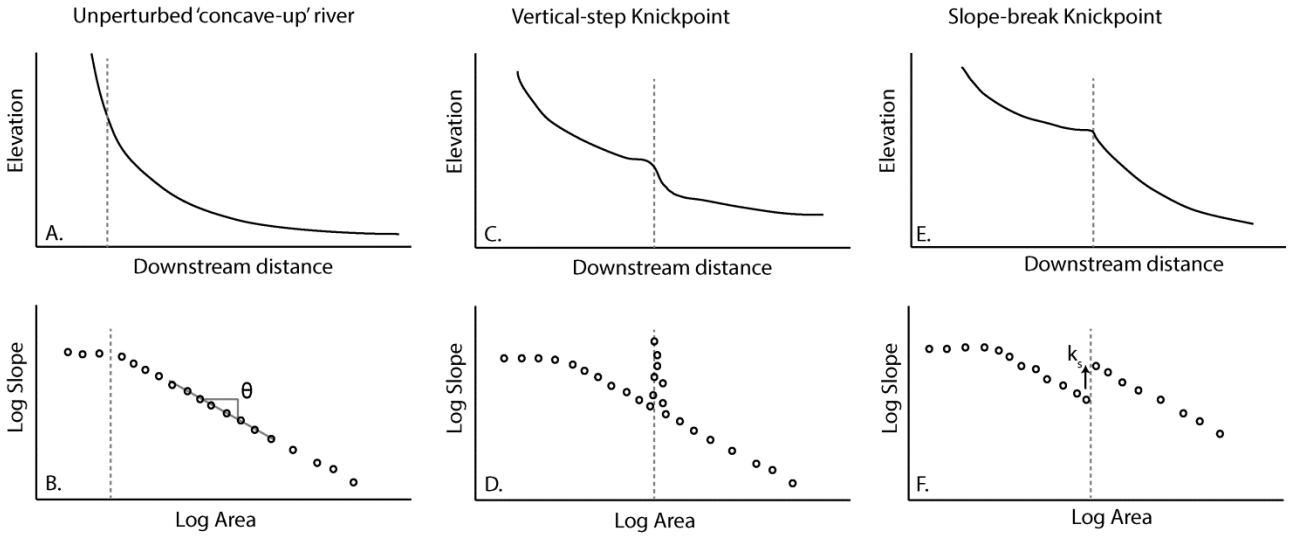

Figure 4. Schematic diagrams showing the river long profile and slope-area plot, respectively, for: a / b) an unperturbed concave-up river, the dashed line indicates the transition from debris flow to fluvial processes, note that downstream of this break.

The temporal and spatial characteristics of the perturbation will determine the fluvial response to the forcing. A discrete event, such as a locally resistant substrate, a debris flow or landslide, will cause a deviation away from equilibrium (Kirby and Whipple, 2012; Walsh *et al*., 2012), generating a 'vertical-step knickpoint' (Kirby and Whipple, 2012) that can be recognised on a slope-area plot as a spike in slope values (Fig. 4). These knickpoints are often anchored in space and have no direct tectonic significance (Kirby and Whipple, 2012).

By contrast, 'slope-break knickpoints' (Kirby and Whipple, 2012) represent a break in the slope-area scaling (Fig. 4) and develop as a response to a persistent change in forcing that drives the fluvial system towards a new equilibrium (Tucker and Whipple, 2002). Such forcing mechanisms may be due to the initiation of faulting or to a change in slip rate along a fault and as such slope-break knickpoints enable the interpretation of tectonics in erosional landscapes (Wobus *et al*., 2006; Kirby and Whipple, 2012). The identification of linear alignments of slope-break knickpoints have led to the recognition of previously unknown geological structures (i.e., Wobus *et al*., 2003; Kirby *et al*., 2003; Kirby and Ouimet, 2011) as well as implying changes in uplift rate across known structures (e.g., Schoenbohm *et al*., 2004; Kirby *et al*., 2007; Hoke *et al*., 2007). Significantly, this class of knickpoint normally migrates upstream at a constant vertical rate (Whipple and Tucker, 1999; Neimann *et al*., 2001) but the horizontal celerity is a primarily a function of drainage area, thus as the size of the drainage area decreases so does the velocity of the knickpoint migration (Whipple and Tucker, 1999; Crosby and Whipple, 2006; Berlin and Anderson, 2007; Harkins *et al*., 2007). Therefore, knickpoints associated with persistent changes in rock uplift and should occur at a constant elevation if they have migrated at a constant rate and assuming that the drainage network was in equilibrium prior to perturbation (e.g., Wobus *et al*., 2006; Harkins *et al*., 2007; Cook *et al*., 2009). However, a number of factors can cause deviations from the idealised response, such as spatial variations in uplift rates, climatic variation or the absence of pre-existing steady-state,

resulting in a dispersion of knickpoint heights and differences in knickpoint celerity (Harkins *et al*., 2007; Boulton and Whittaker, 2009; Schildgen *et al*., 2012; Whittaker and Boulton, 2012; Castillo *et al*., 2013).

Recently, Regalla *et al*., (2013) also recognised that slope-break knickpoints may be localised above stationary variations in rock uplift, such as above ramp-flat transitions along thrusts (. In addition, field studies in New Zealand suggest that the knickpoint elevation can also be a function of catchment drainage areas where knickpoints get pinned at a critical threshold value when the catchment area upstream of the knickpoint gets too small to drive further migration (Crosby and Whipple, 2006). Despite differing controls on formation, knickpoints will separate areas of the landscape responding to the new boundary conditions from areas that have not yet adjusted (Wobus *et al*., 2006; Crosby and Whipple, 2006; Crosby *et al*., 2007). So long as the lower reaches are not oversteepened (where $\Theta > 1$), the steepness index should correlate with rock uplift rates as for steady-state rivers (Kirby *et al*., 2007).

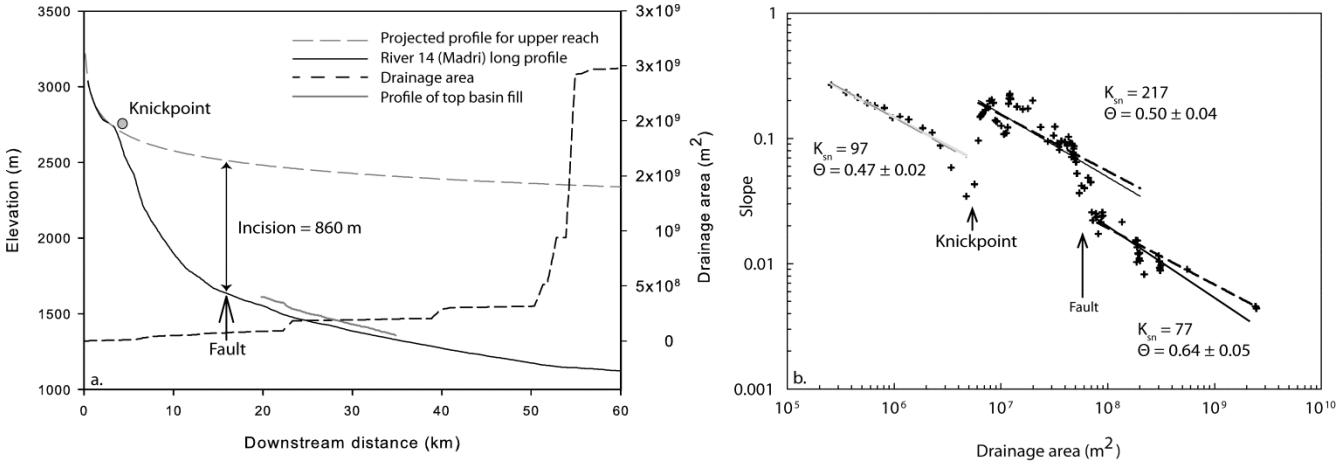

Figure 5. a) River long profile of river 14 showing the parameters used to derive knickpoint height and minimum incision. The dashed line shows the total drainage area and The height of the top basin fill is also indicated by the grey line; b) Slope – area plot for the river 14 derived from a, showing the changes in scaling associated with the knickpoint and thrust front.

Therefore, by analysing the distribution and characteristics of knickpoints it is now becoming possible to discriminate between different modes of formation (i.e., lithologic or tectonic), yield data on erosional responses to relative base level changes (e.g., Clark *et al*., 2005; Harkins *et al*., 2007; Castillo *et al*., 2013) and even to make estimates on the age of knickpoint formation and the rate of fault motion (e.g., Boulton and Whittaker, 2009). Although, distinguishing between tectonic and climatic signals within a transient landscape remains an outstanding challenge for geomorphologists (Kirby and Whipple, 2012).

METHODS

Longitudinal river profiles (draining southwards from the watershed to the confluence with the Dades-Draa River across the SAF) were extracted using a combination of the RiverTools 3.0

programme and the ArcInfo suite of programmes. A hole-filled 3 arc-s Shuttle Radar Topography Mission (SRTM) derived Digital Elevation Model (DEM) with a ~ 90 m ground resolution (USGS, 2006) was chosen. In this case, although the resolution is not sufficient to resolve narrow canyons within the DEM, the SRTM data was found to be of much better quality than the higher resolution ASTER DEM with 30 m resolution. Furthermore, Wobus *et al*. (2006) found little difference between profiles extracted from 90 m DEM compared to 30 m DEMs. DEM data were processed using the Imposed Gradients Plus method, an extension of the imposed gradients method of Garbrecht and Martz (1997) that reduces parallel flow within valley flats. Although, RiverTools automatically fills pits within the DEM when calculating the flow grid, the original DEM can be viewed and areas of poor fit can be identified between the raw and filled DEM. To reduce noise and artefacts in the data the longitudinal profile data were smoothed using a 30 m (vertical interval) moving average filter to remove spikes in elevation. All major river systems were extracted along strike and were only selected where drainage area exceeded 10^5 m^2 (cf. Kirby and Whipple, 2001; Kirby *et al*., 2007). Channel slope, S, and upstream drainage area, A, were calculated over an average of 20 m elevation intervals. Unfortunately, four profiles from two river systems have significant 'flats' due to poor DEM resolution in areas of high relief and deep incision below the resolution of the DEM. These profiles are still used for the analyses but slopes were not calculated over problematic intervals. Collectively, the slope and area data were then used to calculate the channel concavity, Θ, and the steepness index, k_s, through a regression of the logarithms of S and A (Fig. 5). As the concavity determines k_s, we also quote the normalized steepness index, k_{sn}, calculated using a reference concavity, Θ_{ref} (Wobus *et al*., 2006). Θ_{ref} can be determined using the mean of observed Θ values of apparently undisturbed channels in the study area (here Θ = 0.6). However, in principle the differences in k_{sn} do not depend on the Θ_{ref} chosen (Wobus *et al*., 2006) and when Θ_{ref} = 0.6 is applied to the Moroccan river data the errors become much larger than when a standard Θ_{ref} = 0.45 is used. Therefore Θ_{ref} = 0.45 is used in this study as; a) the error is reduced in the resultant k_{sn} value (Table 1), and b) the value is consistent with other studies that use Θ_{ref} = 0.45 (e.g., Wobus *et al*., 2003; 2006; Ouimet *et al*., 2009; DiBiase *et al*., 2009; Cyr *et al*., 2010; Miller *et al*., 2012) allowing for comparison.

Knickpoints were identified based upon observed breaks in scaling on the SA plots (Fig. 5). On rivers where knickpoints were identified, Θ and k_{sn} were calculated separately for channel reaches above and below the knickpoint(s). Knickpoints were also mapped onto the DEM so that any spatial relationships between knickpoint locations and lithological boundaries based upon published maps (Saadi *et al*., 1978) could be identified. Furthermore, the amount of incision was estimated by projecting the river profile downstream of the knickpoint using the derived parameters of best fit steepness (k_s) and concavity derived from Eq. 1 (derived from the a curve fit of slope versus area) and the modern drainage area to calculate slope above the knickpoint. These slopes were then used to project the long profile downstream (c.f., Berlin and Anderson, 2007; Goldrick and Bishop, 2007; Harkins *et al*., 2007; Miller *et al*., 2012; Schildgen *et al*., 2012; Antón et al., 2012). The height of the present profile elevation at the thrust front was then subtracted from the reconstructed profile to give the change in channel elevation resulting from incision (Fig. 5) (Whipple and Tucker, 1999). Errors in the prediction were estimated from the 95% (2σ) prediction bands. Uncertainty in knickpoint elevations were taken as an error of ± 30 m, which has been

determined as the vertical error of SRTM data and used in other studies utilising SRTM data in mountainous areas (Harkins *et al*., 2007; Miller *et al*., 2012).

RESULTS

Twenty one of the 32 river profiles (Fig. 6) analyzed in this study exhibit knickpoints of which 17 rivers have one knickpoint and 4 rivers have two knickpoints. The eleven rivers that do not display knickpoints have concave-up profiles, are distributed along the entire length of the mountain range in the study area and are positioned in-between the rivers that display knickpoints (Fig. 7). These concave-up rivers are often relatively short in length (average of 52 km upstream of Dades confluence), compared to an average of 67 km for rivers with knickpoints, with mean concavity (Θ) equalling 0.64 ± 0.3, over the range of 0.25 - 1.00 (table 1). The normalized steepness index (k_{sn}) of the concave-up rivers also shows variability ranging from 47.5 – 219.0 $m^{0.9}$ (table 1). There does not appear to be any identifiable pattern in the variation of either of these parameters along the strike of the range front but it should be noted that the majority of these concave-up rivers do flow over faults at the range front as do the rivers with knickpoints.

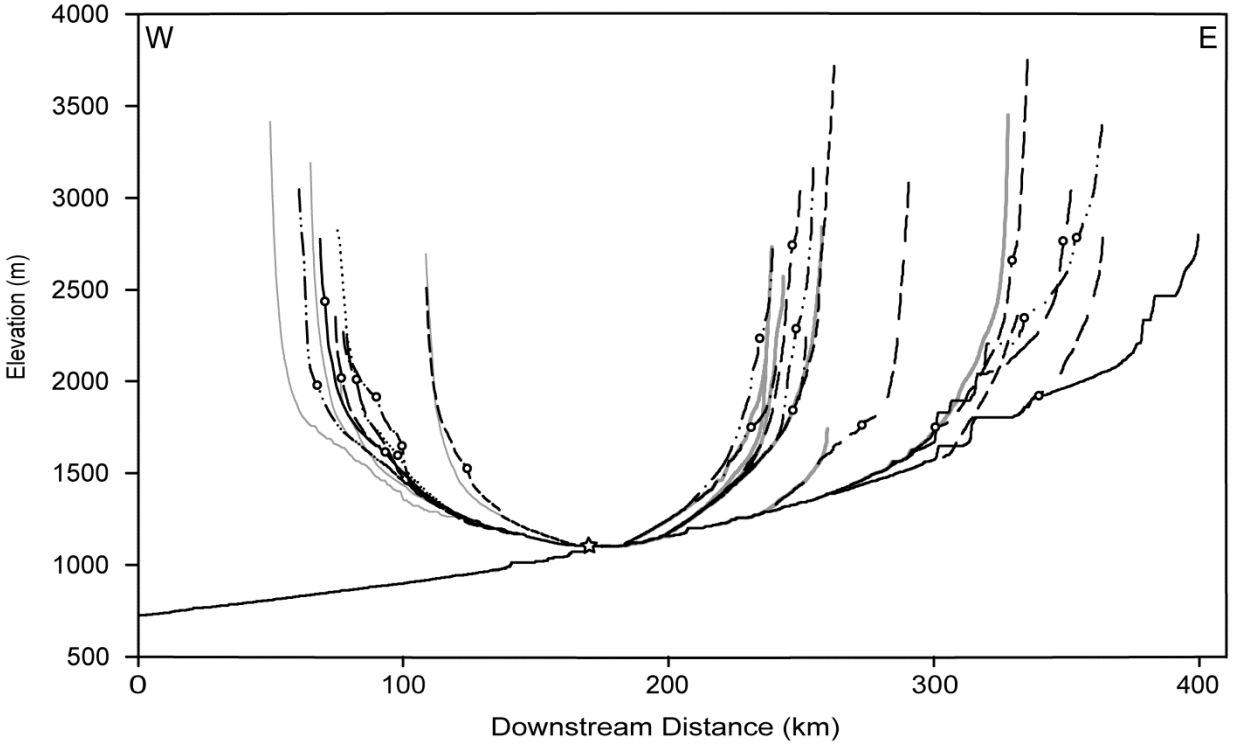

Figure 6. River long profiles of all rivers extracted; solid line is the Dades-Draa River, black dashed lines indicated rivers with knickpoints, and grey solid lines indicate rivers lacking knickpoints. The star shows the knickpoint associated with the Dades-Draa.

By contrast, 21 rivers exhibit a knickpoint or multiple knickpoints. Although the morphologies of the rivers show some variation they share a number of characteristics (Fig. 8). The majority of rivers exhibit slope-break morphology when S and A are plotted on a slope-area plot (Fig. 8), with k_{sn} and Θ values higher below identified knickpoints (i.e., there is steepening across the knickpoint) than above. By contrast, a few rivers exhibit vertical-step knickpoints where Θ and k_{sn} show minimal or no change above and below the knickpoint.

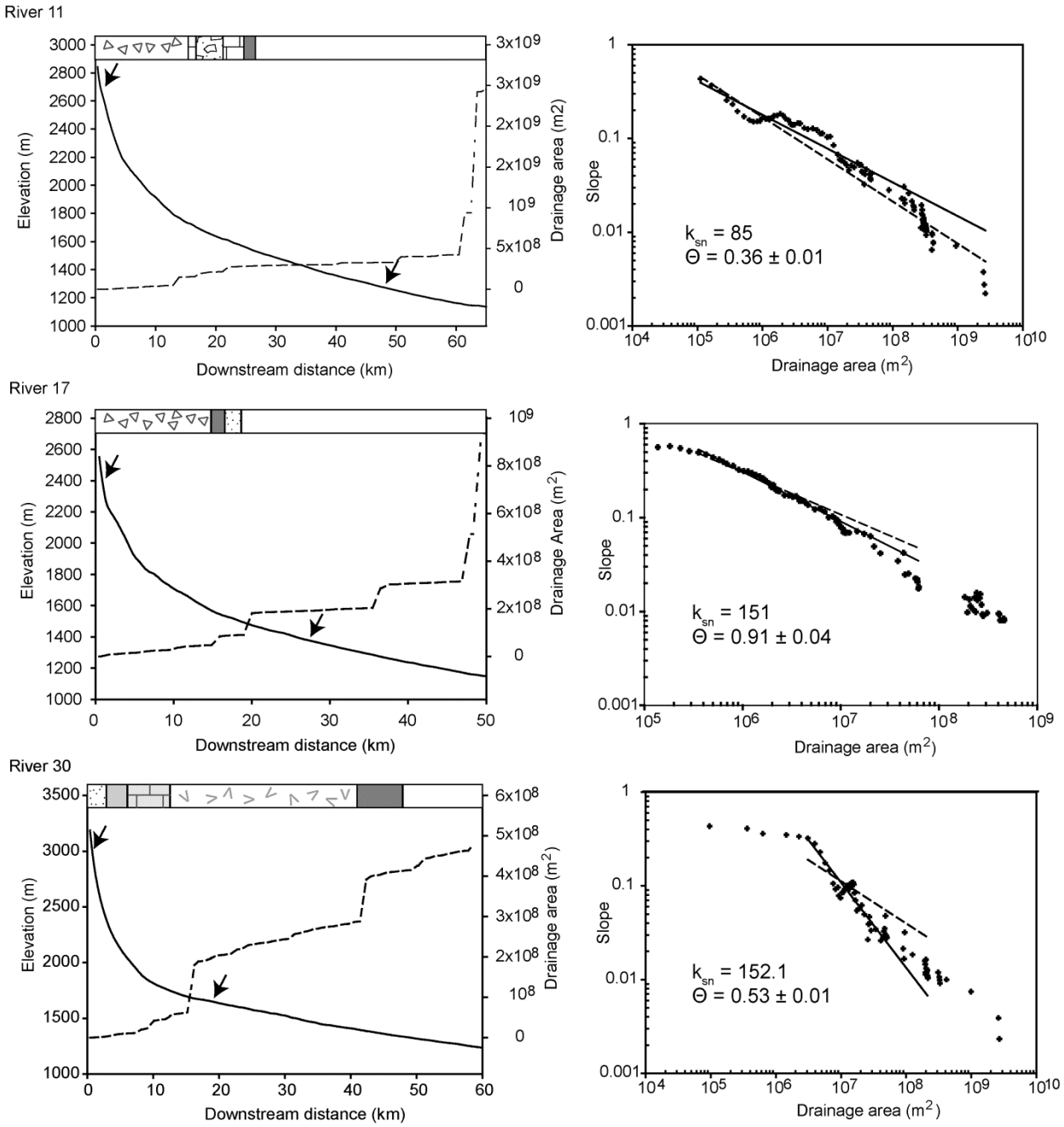

Figure 7. Representative examples of concave-up river profiles (solid lines) exhibiting consistent power-law scaling between drainage area and slope. Rivers profiles and drainage areas (dashed lines) were extracted from the SRTM DEM (USGS, 2006) and each river is labelled with a number that corresponds to those shown in figure 3. Arrows mark upstream and downstream limits of data used for regression analysis on the slope-area plots; the concavity ,Θ, and normalised steepness index, ksn, where Θ = 0.45 are also shown on the slope area plots. At the top of the long profile plot is a bar showing the lithology downstream (for key see Fig. 2)

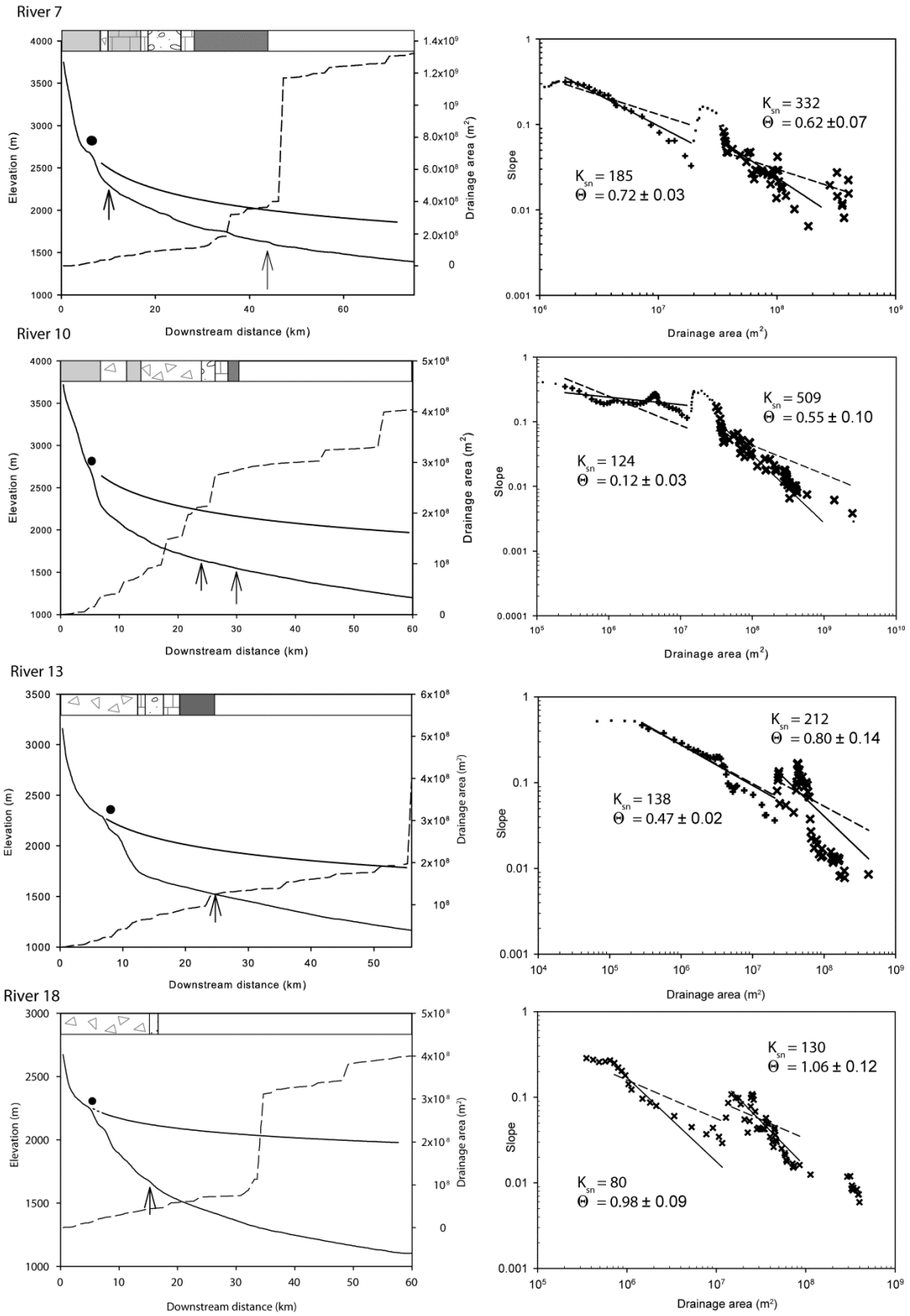

Figure 8. Representative examples of river profiles (solid lines) that exhibit knickpoints (circles) and segmented power-law scaling characteristic of slope-break knickpoints where ksn increases downstream, each river is labelled with a number that corresponds to to those shown in figure 3. Reconstructed relict profiles and position of the frontal thrust (arrow) are also shown. At the top of the long profile plot is a bar showing the lithology downstream (for key see Fig. 2).

The presence of knickpoints on the long-profiles and SA plots, combined with documented evidence of gorges and high relief (Stokes *et al,*. 2008), can be explained as a result of transient fluvial incision across the region (i.e., Wobus *et al*., 2006; Berlin and Anderson, 2007; Harkins *et al*., 2007; Whittaker *et al.*, 2007; 2008; Kirby and Whipple, 2012; Miller *et al*., 2012). In order to determine the controls on and interpret the significance of the knickpoints identified along the southern margin of the High Atlas, firstly the relationship to lithological boundaries and the horizontal and vertical distribution of the knickpoints will be examined . Followed by an assessment of other potential mechanisms of formation (i.e., river capture and uplift), finally the tectonic implications for the present of knickpoints will be considered.

Spatial distribution of knickpoints

When the distribution of knickpoints is considered in relation to lithological contacts and faults, it can be observed that the vast majority of knickpoints do not lie on major lithological contacts (Fig. 2) and that knickpoints occur in a range of lithologies from Silurian and older schists, Permo-Triassic basalts to Jurassic limestones and sandstones upstream of the thrust front and mapped faults.

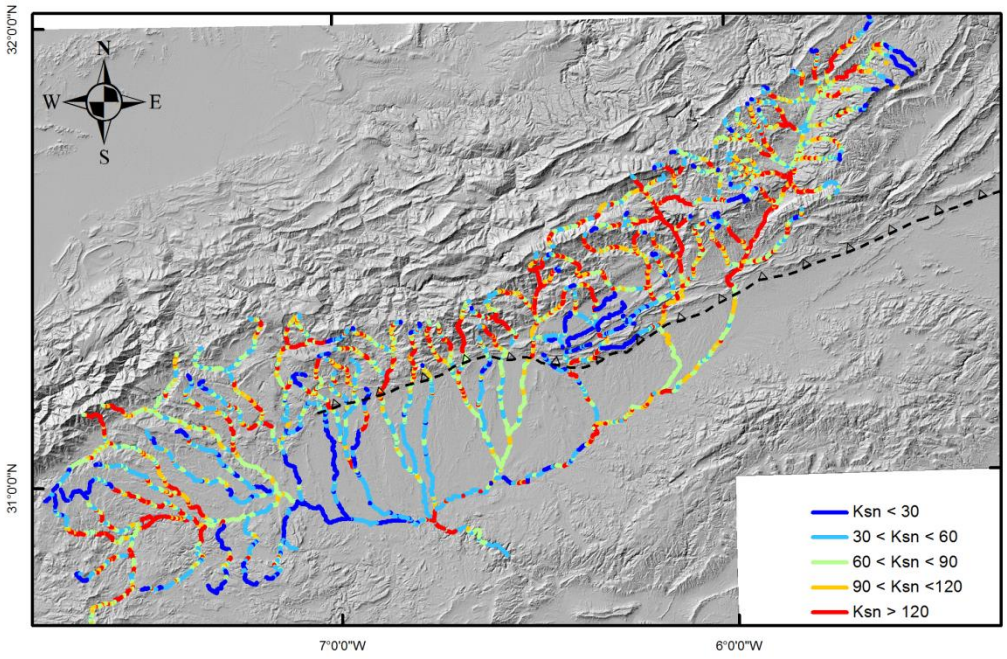

Figure 9. Grey scale hillshade of the study area with the drainage network coloured by variation of ksn downstream.

However, some knickpoints do fall near to boundaries and all rivers cross multiple lithological boundaries but given the complex geological nature of the mountain belt this is not unexpected. Furthermore, when boundaries are traced along strike, knickpoints can be observed along some rivers yet not along others crossing the same boundary (i.e., the Lower Jurassic [Pleinsbachian] to Upper Cretaceous boundary in the west of the study area). Yet these

observations cannot rule out changes in the strength of rocks due to intraformational variation, geological structures or unrecognised features to the scale of available maps. Compelling evidence against a dominant lithological control on knickpoint location comes from the SA plots that exhibit slope-break relationships and demonstrate increasing k_{sn} below knickpoints (Figs. 8 and 9). For example, along river 18 (Fig. 8; a tributary of the Izerki) k_{sn} above the knickpoint is 80 $m^{0.9}$ while below the knickpoint k_{sn} = 130 $m^{0.9}$, the plot shows a clear step (Fig. 8) and the concavity index is similar above and below the knickpoint. Lithological resistance would not be expected to increase k_{sn} downstream as this parameter is sensitive to uplift not rock strength (Synder *et al*., 2001; Wobus *et al*., 2006) indicating that these knickpoints are unlikely to be the result of a change in bedrock resistance.

In the western portion of the basin, a few knickpoints are closely associated with geological boundaries (i.e., the Upper Cretaceous limestones to Eocene sandstones and conglomerates boundary). When the slope-area plots are considered for rivers 25, 27 and 29 the SA plot resembles a vertical-step knickpoint (Fig. 10). For example, river 25 displays several peaks in the SA plot that correlate with knickpoints on the long profile (Fig. 10). These knickpoints are located upon Permo-Triassic basalts or at the boundary between Cretaceous and Jurassic limestone. The k_{sn} above and below the knickzones are the same within error for river 25, supporting a local control on river morphology. River 29 also shows at vertical-step knickpoint at this boundary (Fig. 10). River 27 is a tributary to river 25 and shows a spike in slope values typical of vertical-step relationships at the boundary between Eocene clastics and Cretaceous Limestone (Fig. 10). In this case the k_{sn} downstream is higher than k_{sn} above the main knickpoint, possibly suggesting that some knickpoints may reflect combined lithological and base-level effects.

We can now distinguish between knickpoints with no obvious lithological control and knickpoints that indicate lithological influence. When the spatial distribution of knickpoints is considered in relation to the trend and structure of the High Atlas, it is observed that the majority of knickpoints align along a trend sub-parallel to the strike of the mountain belt (Figs. 2 and 3) and upstream of the thrust front. Only a few knickpoints in the west of the study area deviate from this trend; it is these rivers that appear to have a lithological influence to the position of the knickpoints, or the knickpoints are located very close to the catchment watershed. Rivers 8 and 12 also lie off the along strike trend but these have smaller catchments that may be retarding the progress of knickpoints along the reach. Finally, there appears to be no relationship between the location of knickpoints and major stream confluences (i.e., Figs. 8 - 9).

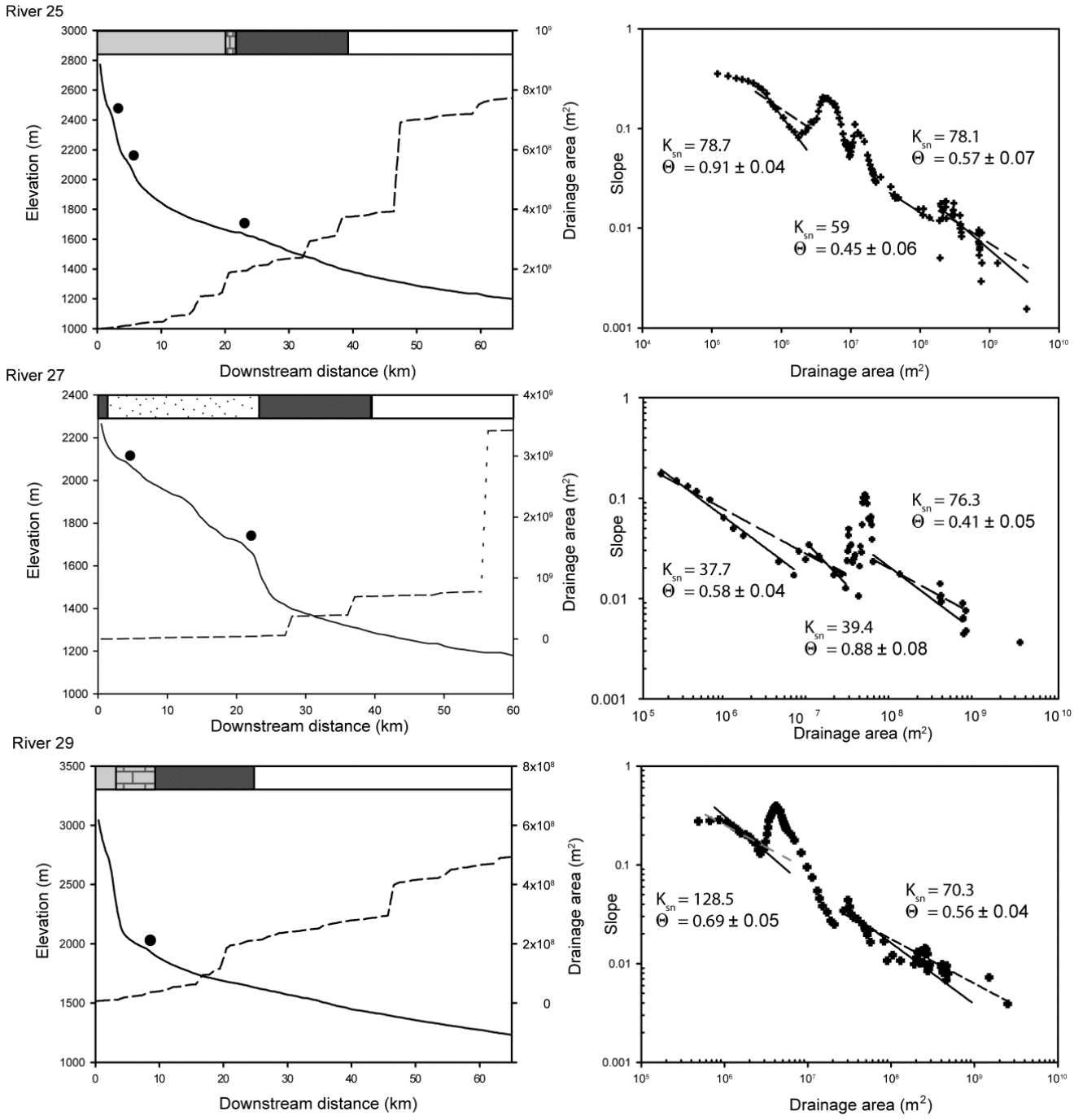

Figure 10. River profiles from the study area that exhibit knickpoints (circles) and segmented power-law scaling characteristic of vertical-step knickpoints where ksn does not increases downstream, each river is labelled with a number that corresponds to those shown in figure 3. At the top of the long profile plot is a bar showing the lithology downstream (for key see Fig. 2). Note that on the topographic long profile some knickpoints can be less obvious than others yet can be clearly discerned on the SA plot, i.e., river 25.

Horizontal and vertical distribution of knickpoints

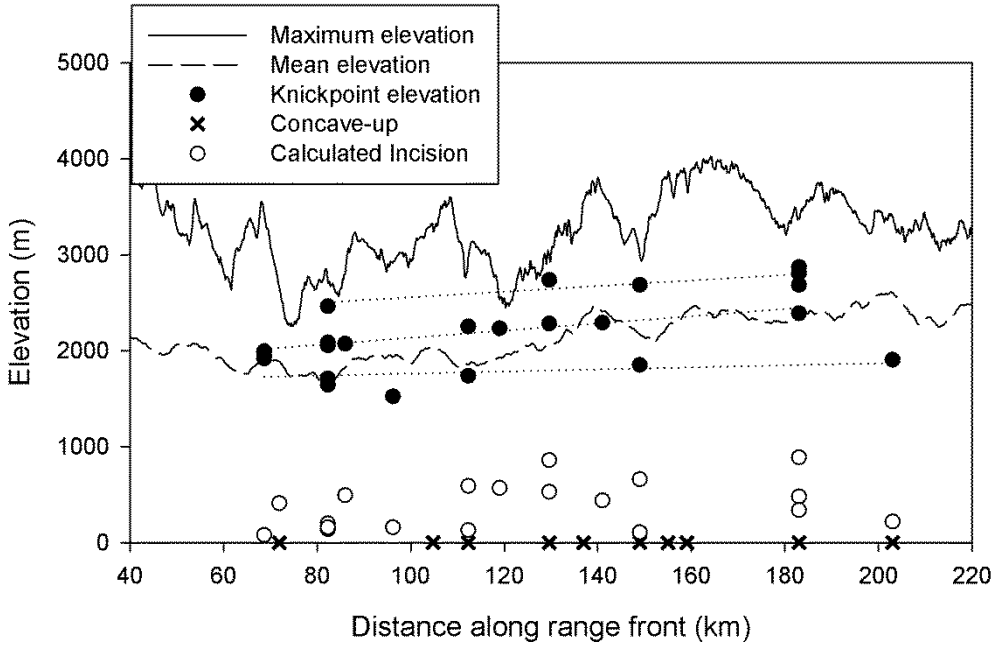

Figure 11. Knickpoint elevations (above mean sea level) and river incision plotted with maximum and average swath profiles of the range topography. Dotted lines shows potential vertical distribution of knickpoints into three elevation bands, analysis of horizontal knickpoint retreat distance against drainage area (Fig. 12b) shows that all knickpoints belong to the same generation and show a range in distribution.

Figure 12a shows that there is no relationship between catchment drainage area and knickpoint elevation, and lithological and non-lithologically controlled knickpoints plot together. By contrast, horizontal retreat distance does scale with catchment area where rivers with larger catchments have knickpoints further upstream (Fig. 12b). The horizontal knickpoint retreat distance was measured from the mapped location of the frontal thrust, or the lithological boundary between the foreland basin sediments of the Ouarzazate Basin and the older rocks forming the High Atlas where a frontal thrust is not present at the surface. This finding is in agreement with other studies (e.g., Bishop *et al*., 2005; Crosby and Whipple, 2006; Harkins *et al*., 2007; Jansen *et al*., 2011; Castillo *et al*., 2013) that have shown that the horizontal knickpoint retreat distance scales with total catchment area in fluvial systems, demonstrating that knickpoint retreat rate is a function of river discharge. Interestingly, the rivers where a lithological influence on knickpoint form has been implicated plot in the same field as the other knickpoints (Fig. 12). This suggests that although the present location of the knickpoints is at a lithological boundary these knickpoints may not be caused primarily by the lithological variation. Limited lithological or structural control on knickpoint formation has also been demonstrated in the Scottish Highlands (Jansen *et al*., 2011; Castillo *et al*., 2013).

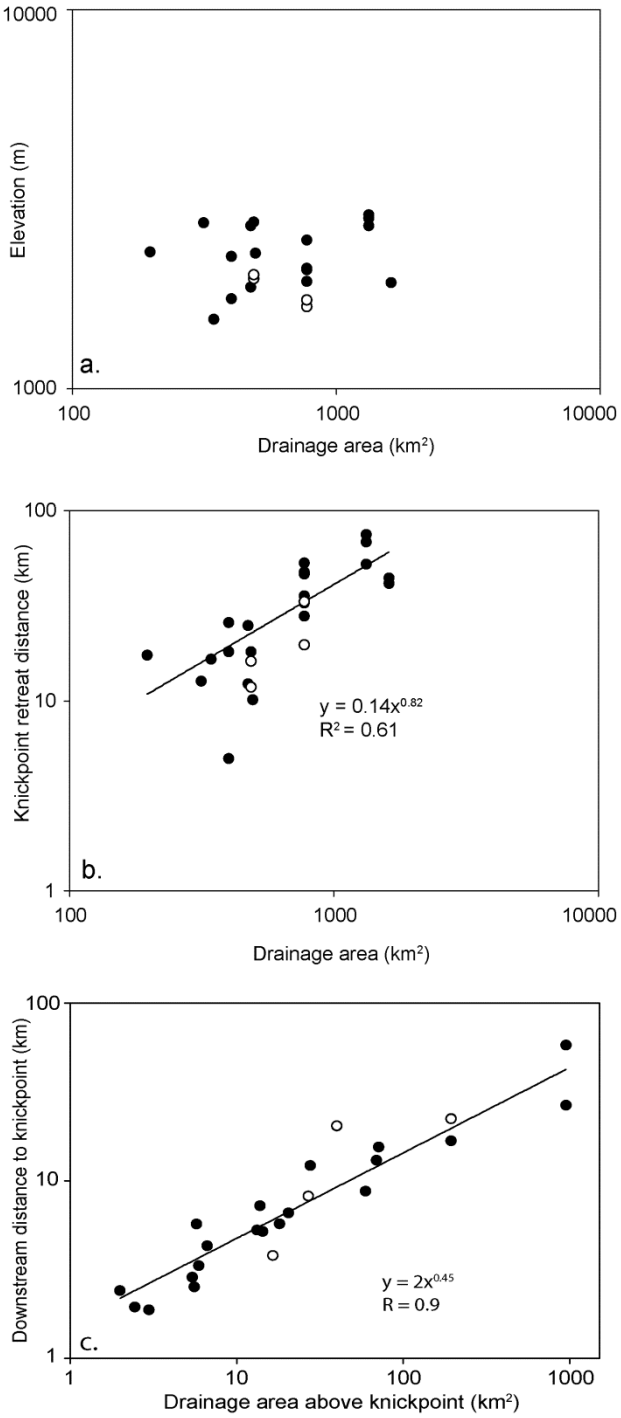

Figure 12. Graph of total drainage area versus elevation of the knickpoint, white circles indicate rivers where lithology plays a role in knickpoint position; b) Graph of total drainage area versus the distance the knickpoint has retreated from the thrust front. A linear regression yields the best fit power-law equation: y = 0.14A0.82 with R2 = 0.61; c) Graph of drainage area (A) above knickpoint versus downstream distance from the divide (y) to the knickpoint. A linear regression yields the best fit power-law equation: y = 2A0.45 with R2 = 0. 9.

These observations on knickpoint elevation and retreat distance appear to contradict each other, on the one hand the knickpoint elevation indicates multiple knickpoint generations while analysis of horizontal retreat distasnce indicates only one generation of knickpoints. Although, Neimann *et al*. (2001) predict that the elevations of knickpoints that were generated at the same time should be the equal, in practice this is not always observed due to the presence of a threshold drainage area (Crosby and Whipple, 2006), inherited long-profile characteristics (Castillo *et al*., 2013), sediment flux (Jansen *et al*., 2011), differential uplift rates along strike (Boulton and Whittaker, 2009) or the presence of lithologies resistant to erosion (Berlin and Anderson, 2007). Whereas, the horizontal retreat distance appears to always scale with drainage area (e.g., Bishop *et al*., 2005; Crosby and Whipple, 2006; Harkins *et al*., 2007; Jansen *et al*., 2011; Castillo *et al*., 2013), and thus knickpoints of different generations ought to show different scaling between catchment area and retreat distance.

Therefore, the knickpoints in the High Atlas of Morocco are interpreted to have formed synchronously based upon the knickpoint retreat distance scaling with drainage area.

Finally, the relationship between downstream distance (measured from river profiles) and the drainage area above the knickpoint is also considered. These parameters can be fitted by a power-law function with an exponent of 0.45 (Fig. 12c), thus exhibiting scaling behaviour consistent with Hack's Law for stream profiles (Willemin, 2000). A similar relationship was recorded by Miller *et al*. (2012) for rivers in Papua New Guinea demonstrating that the knickpoints lie within channel networks rather than

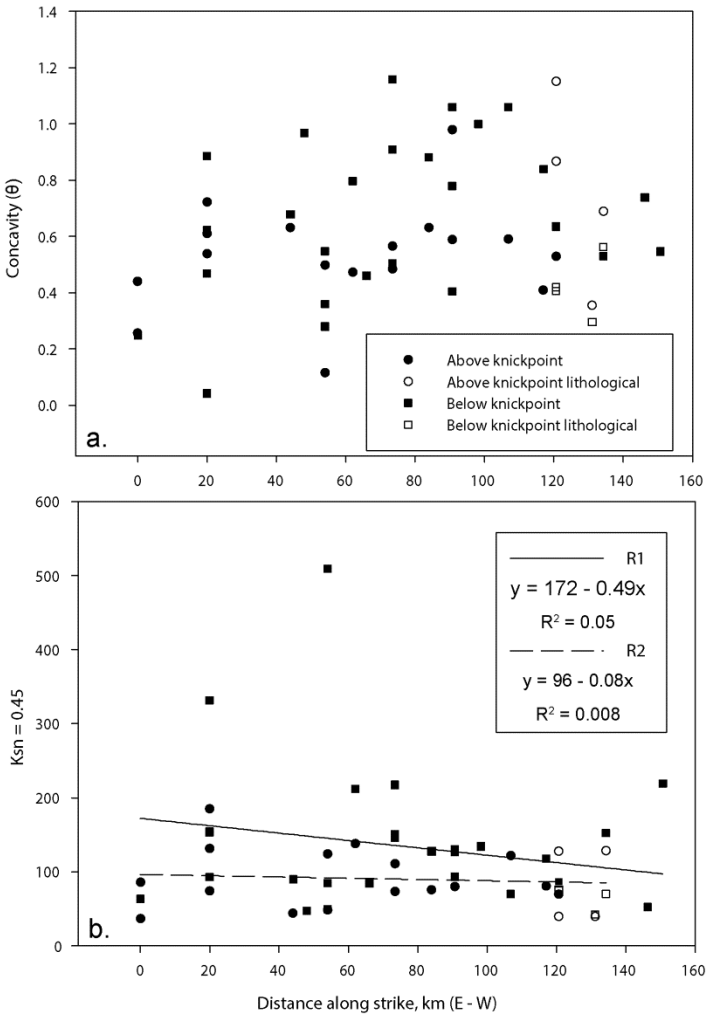

Figure 13. A) Concavity indices (Θ) for each river segment plotted along the strike of the mountain front. B). Ksn values (Θref = 0.45) for each river segment; symbols are the same for both graph.

at the hillslope – channel transition (e.g., Crosby and Whipple, 2006; Harkins *et al*., 2007). Furthermore, as there are a range of drainage areas upstream of the knickpoint it does not appear that the knickpoints have reached a threshold drainage area indicating that the landscape is still transiently responding to the change in boundary conditions that formed the knickpoints (Crosby and Whipple, 2006; Berlin and Anderson, 2007).

Therefore, the spatial variations in the transient response observed in the rivers flowing southward across the SAF in the absence of strong lithological control are most easily explained by a relative lowering of base-level attributable to either stream capture or an increase in rock uplift.

Longitudinal profile analysis

Using the findings above, we consider that the lowest knickpoint on each river formed during a single base-level fall event and thus channel segments above and below this knickpoint can be correlated. Rivers that have a lithological influence on knickpoint position (including those exhibiting two knickpoints) are again considered separately.

Concavity indices are generally higher downstream of knickpoints (mean Θ = 0.66) than above (mean Θ = 0.53), although the reverse is true for lithologically controlled knickpoints, 0.56 and 0.77, below and above the knickpoint respectively. The reaches above the higher knickpoint, where present, have a mean Θ of 0.75. These means are high but not unusually so (Whipple, 2004; Kirby and Whipple, 2012). No along strike trends are evident in concavity either above or below the knickpoint (Fig. 13a). Variation in concavity has been attributed to changes in rock strength (Duvall *et al*., 2003) with lower concavities in weaker rocks.

Upstream of knickpoints, mean k_{sn} equals 93 $m^{0.9}$ spanning a range from 37 to 185 $m^{0.9}$. The reach downstream of knickpoints typically has a higher k_{sn}, the mean is 145 $m^{0.9}$, over a range of 50 – 509 $m^{0.9}$ consistent with steepening below the knickpoint as a result of base-level fall. For individual catchments the river is always steeper downstream by a factor of 1.2 to 4. There appears to be no along strike variation in k_{sn} above the knickpoint; however, k_{sn} values below the knickpoint exhibit a weak west to east increase in k_{sn} (Fig. 13b).

The long profile downstream of the knickpoint was reconstructed downstream using extracted values for k_s and Θ (cf., Berlin and Anderson, 2007; Miller *et al*., 2012). k_{sn} was not used as this proved to be a poor fit in most cases. The modern elevation profile was then subtracted at the mountain front to give an estimate of incision (Fig. 5). The mean incision estimate is 430 ± 248 m (excluding lithological knickpoints) with a maximum incision of 900 m. When along strike variations are considered no strong relationship is observed, however, when the lithologically influenced knickpoints are included in the dataset there is a weak west to east increase in the estimated incision pattern (Fig. 13c). Furthermore, there is a west to east increase in the elevation of the knickpoints (Fig. 11).

There are not enough data to undertake meaningful analyses on the higher knickpoints, but these may represent an earlier transient response to a landscape perturbation that has now almost completely migrated through the channel system.

DISCUSSION

Knickpoint formation as a result of river capture?

Pastor *et al*. (2012b) identified piedmont stream capture events along seven of the rivers studied here, these were (Fig. 3): the Amaragh (river 23); the Tanjout (River 18, two capture events); the Madri (two capture events on the trunk river effecting rivers 14, 16, 17), and the Tabia (river 13). Pastor *et al.* (2012b) also identified capture events on a number of streams that are confined to the foreland basin, and are not considered here. The documented capture events result in a number of stepped fan pediments along many rivers, primarily as a result of intrinsic processes (e.g., erosion, sediment supply and transport), although Pastor *et al*. (2012b) do not rule out tectonic and climatic control on their formation. However, given that these river capture events have been dated to have taken place multiple times throughout the Late Pleistocene and Quaternary (Pastor *et al*., 2012b) on an 100 ka timescale, these intrinsic river captures cannot explain the single knickpoint generation observed upstream in the hinterland.

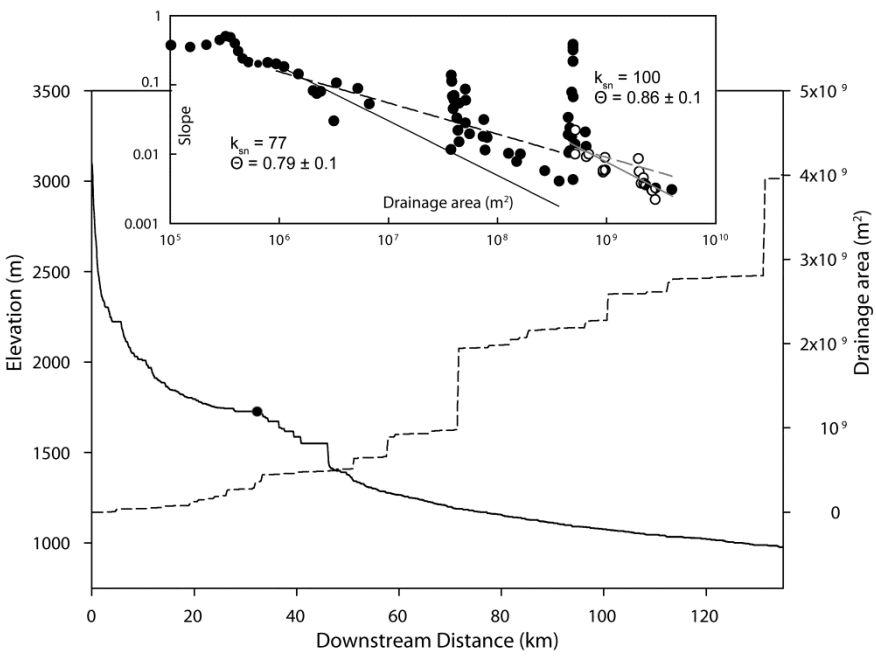

Figure 14. River long profile (elevation against downstream distance) of the Todra river (solid line) and drainage area downstream (dashed lines), the knickpoint is indicated with a solid circle. Inset shows the slope-area plot, steps in the long profile create noise in the data but a vertical step in the ksn values can be determined across the knickpoint.

However, the Ouarzazate Basin has undergone a continent-scale river capture event, as the

Ouarzazate Basin was internally draining until the River Draa captured the Dades drainage system. This event is poorly dated but likely occurred ≤ 300 ka (Arboleya *et al*., 2008) and resulted in the incision and erosion of the foreland basin fill by 100 - 150 m, as such this event could be a mechanism for base-level fall leading to knickpoint formation. If this were the case a number of broad predications can be made for the resulting form of rivers and knickpoints upstream of the capture site. Firstly, knickpoints should be present in all of the drainages upstream of the capture site (i.e., all the rivers studied here), apart from streams with small drainage areas where the knickpoint may have already migrated through the system. Second, as the magnitude of base-level fall is controlled by the capture event, the resulting steepness (k_{sn}) below the knickpoint will depend on the distance from the knickpoint to the capture point, therefore rivers central to the capture point will have steeper lower reaches than rivers that drain further along strike. Thirdly, the calculated incision from profile-reconstructions should reflect the magnitude of incision. Additionally, the reconstructed river profile should grade to the top basin fill of the Ouarzazate Basin as there is no differential uplift between the foreland and hinterland in this model. Finally, rivers to the east and therefore outside of the Ouarzazate Basin should not exhibit a knickpoint as rivers, such as the Todra (immediately east of the Dades), have not been captured by the Draa and discharge directly into the Sahara Desert.

Each of these points can be tested using the observations made on the studied rivers. The first predication is that all rivers should exhibit knickpoints, unless the river has a small drainage area. Knickpoints are not present on all of the studied rivers but those that lack knickpoints do not have significantly drainage areas smaller than those that do (Table 1). Secondly, rivers should be steeper downstream and the rivers most proximal to the capture will be the steepest. Although, rivers are steeper below knickpoints, rivers 18-20 that are central to the capture site are not the steepest rivers, indeed there is a slight (although not significant) west to east increase in steepness inconsistent with this prediction (Fig. 13b). Thirdly, estimates of incision should be consistent with the pre-capture base level (taken as the top basin fill terrace surface); however, the projected profiles lie substantially above the height of the top basin fill terrace surface (Fig. 5). Furthermore, incision amounts vary considerably and also exhibit a slight west to east increase in estimated incision. Fourthly, Figure 14 shows the river long profile and SA plot for the River Todrha, the long profile clearly shows a knickpoint 32 km downstream correlating with a break in scaling on the SA plot and an increase in k_{sn} below the knickpoint from 77 $m^{0.9}$ to 100 $m^{0.9}$, as this river is not part of the Dades-Draa catchment this knickpoint cannot have formed through this capture event. Significantly, a knickpoint can also be observed on the long profile for the Dades-Draa River (Fig. 6: star) near the capture area suggesting that this wave of incision has not migrated far into the basin.

Furthermore, although there are very few studies that investigate rates of capture related incision, examples such as Stokes et al., (2002) describe a 90 m capture related base level fall that has transmitted a maximum of 20 km upstream from the capture site in 100 kyr. Despite the uncertainties in the timing of the Dades-Draa capture, it seems unlikely that any capture related base-level lowering has propagated upstream out of the Ouarzazate Basin into the fold-and-thrust front regions of the High Atlas Mountains. Therefore, the evidence does support the capture of the Dades by the Draa as the mechanism for knickpoint formation.

Knickpoint formation as a result of uplift?

Having ruled out other mechanisms for knickpoint development, given that the reconstructed channel profiles project above the relict fan surfaces at the top of the basin fill, as well as the modern river base-level, and that the mountain front is faulted we attribute the knickpoint formation to an increase in rock uplift. But do the knickpoints represent a transient response to an increase in slip-rate along a planar fault system resulting in relative base-level fall or could these knickpoints be localised above a flat-ramp transition on the thrust front? Regalla *et al*., (2013) demonstrated that in the Tohoku Arc (Japan) two knickpoints develop as a result of the subsurface geometry of the thrust front where changes in the rate of uplift across a flat-ramp transition causes a steady-state convexity to form above the boundary in uplift domains; a second transient knickpoint migrates upstream at the initiation of faulting. This does not appear to be the case in the High Atlas as the position of the knickpoints does not correlate to the position of fold axes, which should be present up to maximum of 5 km towards the hinterland from the frontal thrust zone based upon current mapping (Saadi *et al*., 1978; Beauchamp *et al*., 1999; El Harfi *et al*., 2006).

By contrast, knickpoints developing above a thrust with a planar geometry will be transient in nature, forming due to the initiation, reactivation or acceleration of uplift along the fault. In this case the magnitude of fluvial incision and elevation of knickpoints should be consistent with independent controls on the nature of the uplift. Babault *et al*. (2008) using a range of geological observables argue that the main phase of uplift in the High Atlas took place during the Plio-Quaternary with ~ 1000 m of surface uplift generated. This study shows that knickpoints indicate a mean channel incision of 430 m and a maximum of ~ 1000 m. Although, the mean only represents ~50% of the total uplift previously proposed, the maximum incision calculated here does correlate with the 1000 m of surface uplift calculated by Babault *et al*. (2008). Further constraints on fluvial incision rates and timing of faulting are not possible at this time but previous studies have constrained the geomorphic response times of fluvial landscapes to $10^{5\text{-}6}$ years (Snyder *et al*., 2000; Whittaker *et al*., 2007; Whittaker and Boulton, 2012). Collectively, our data and other published analyses suggest that the initiation of the transient fluvial response was owing to an acceleration (or initiation) in uplift during the Plio-Quaternary in the High Atlas Mountains along a planar fault.

The spatial pattern of uplift along the mountain front can be analysed using the steepness indices and transient incision. Theoretical and empirical studies of the relationship between channel steepness and incision indicate that there is a positive relationship between these variables and that greater incision and steeper channels occur in areas of higher uplift and erosion (Kirby and Whipple, 2001; Snyder *et al*., 2001; Whipple, 2004; Kirby *et al*., 2007). Although, k_{sn} also varies with precipitation, arid and semi-arid landscapes appear to be relatively insensitive to precipitation (D'Arcy and Whittaker, 2014) and given that precipitation is primarily controlled by altitude with no strong longitudinal gradients across the area (Cappy, 2006), k_{sn} is likely to be primarily responding to uplift in this case.

Comparison with previous studies shows that k_{sn} values cannot be directly converted into absolute uplift rates, for example Snyder *et al*., (2000) showed for Southern California that high uplift rates of 3-4 mm yr^{-1} correlated with higher k_{sn} values > 71 and lower uplift rates of < 1 mm

yr^{-1} corresponded to k_{sn} of < 71. Similarly, Kirby *et al*., (2003) showed k_{sn} > 80 for high uplift (1- 3 mm yr^{-1} areas in the Himalaya, and low k_{sn} (< 60) where uplift rates are ≤ 1 mm yr^{-1}. Yet, Duvall *et al*., (2004) in California recorded a maximum k_{sn} of 31 $m^{0.9}$ where uplift rates are ~ 5 mm yr^{-1}. In addition, there is the issue that in some studies there appears to be a linear relationship between steepness and uplift/incision (i.e., Kirby *et al*., 2003; Harkins *et al*., 2007), while other studies observed non-linear relationships between channel steepness and erosion rates (i.e., Duvall *et al*., 2004; Ouimet *et al*., 2009). Although k_{sn} is not directly convertible to uplift rates, given that both k_{sn} and incision estimates (Fig. 13) exhibit a small increase towards the east, as do the elevation of the knickpoints, these collectively suggest that rock uplift rates may slightly increase along the strike of the mountain front from west to east. This pattern is consistent with previous estimates of uplift derived from terraces in the foreland basin (i.e., Arboleya *et al*., 2008).

Tectonic implications

These results have two significant implications for the tectonic evolution and structure of the southern margin of the High Atlas Mountains.

Firstly, two main models for the timing of uplift have been proposed. Missenard *et al*. (2006) suggest that thermal uplift due to lithospheric thinning took place in the Middle Miocene overprinting already elevated topography formed as a result of tectonic shortening. Teson and Teixell (2008) also argue that the Middle Miocene was the main period of topographic growth but as a result of tectonic compression and thrust faulting. This model of Middle Miocene mountain growth is supported with geological evidence on the timing of sediment deposition in the Ouarzazate Basin (Teson *et al*., 2010) and apatite fission track analysis (Balestrieri *et al*., 2009). However, the proposition that current elevations were formed in the Miocene is at odds with other geological constraints on uplift that indicate two pulses of surface uplift have occurred, one > 25 Ma and a more substantive uplift in the Plio-Quaternary (< 5 Ma) (El Harfi *et al*., 2001; 2006; Babault *et al*., 2008). Given that fluvial response times to perturbations are often in the order of a 1 – 5 million years (Whittaker and Boulton, 2012) and the projected amount of fluvial incision is on the order of 1000 m, it is likely that these rivers are responding to Plio-Quaternary not Middle Miocene uplift and resultant relative base-level fall causing the observed transient response in the rivers draining the High Atlas Mountains. The proposed slight eastwards increase in presumed rock uplift also correlates with observations of increased tectonic shortening to the east (Teixell *et al*., 2003). Therefore, this geomorphological study favours a Plio-Quaternary timing for the development of the present elevation of the High Atlas Mountains but does not rule out an earlier phase of uplift in the Early to Middle Miocene.

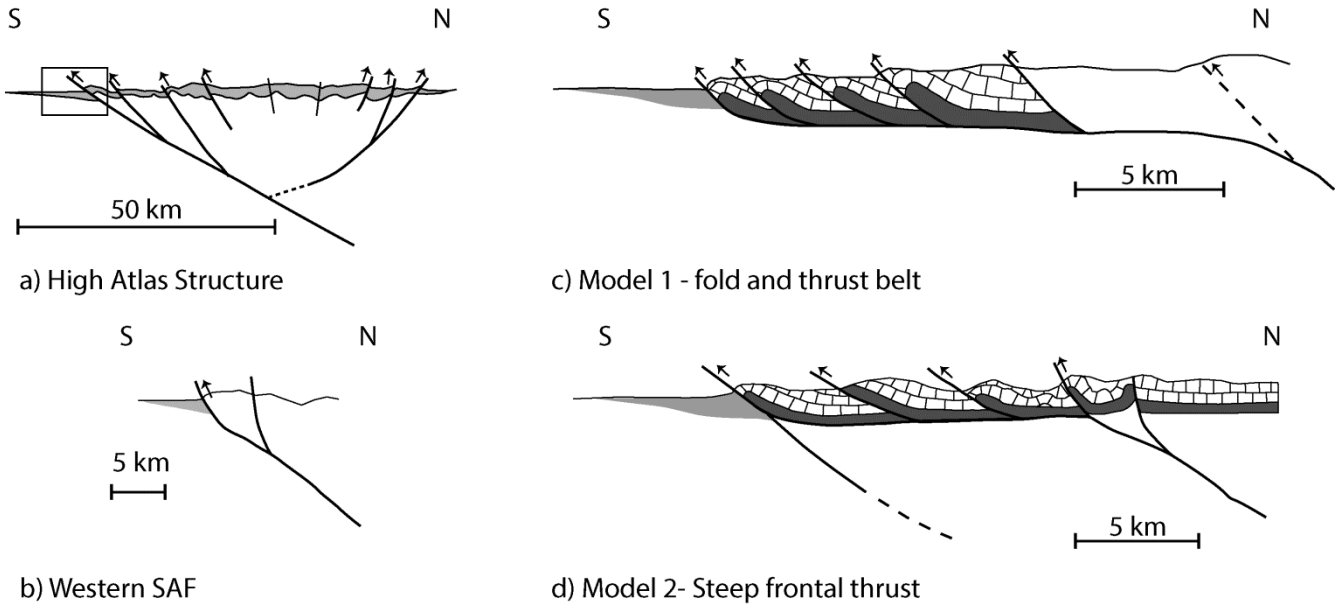

Figure 15a) Sketch cross-section across the whole Atlas Mountains showing bivergent structure resulting from inversion of a Meoszoic rift system, after Babault et al., (2012). Box shows the area shown in more detail in b-d. b) Cross-section showing the structure of the SAF in the west of the Ouarzazate Basin (in the area of rivers 13-23) interpreted as a high angle reactivated normal fault. By contrast, for the eastern part of the basin (in the area of rivers 1 – 8) two models have been proposed – c) a fold and thrust belt with a reactivated normal fault forming an out-of-sequence thrust (i.e., El Harfi et al., 2001; Beauchamp et al., 1999; Teson and Texiell, 2008) or d) a fold and thrust belt bounded by high-angle faults (i.e., Barbero et al., 2007; Babault et al., 2012; Arboleya et al., 2004).

Secondly, our results suggest that the geometry of the fault responsible for the landscape uplift has a planar rather than ramp-flat morphology, which has important implications for the structure of the SAF. In general, the SAF is considered to be a relatively simple structure in the western part of the Ouarzazate Basin (Fig. 15b), consisting primarily of a high-angle reverse fault that initially developed during Mesozoic rifting and was subsequently reactivated to accommodate thick-skinned deformation (Beauchamp *et al*., 1999; El Harfi *et al*., 2001; 2006; Frizon de Lamotte *et al*., 2009). Thin-skinned low-angle faults, forming the thrust front, wedge-top basins and accommodating much of the crustal shortening have propagated at the southern margin of the Atlas Mountains further to the east (where the Dades and M'Goun rivers cross the SAF); these faults have been clearly imaged in seismic lines (Beauchamp *et al*., 1999). Although, offset Quaternary terraces in the Ouarzazate Basin suggest that active thrusting is occurring at the thrust front and may have stepped forward into the foreland basin (i.e., Arboleya *et al*., 2008; Pastor *et al*., 2012a), Beauchamp *et al*., (1999) consider that out-of-sequence thrusting has stepped active faulting back into the fold-and-thrust belt onto a reactivated and inverted normal fault (Fig. 15c). Furthermore, alternative models suggest the presence of a high-angle fault at the boundary between the High Atlas and the foreland basin (Fig. 15d; Barbero *et al*., 2007; Babault *et al*., 2012; Arboleya *et al*., 2004). The presence of a significant high-angle structure at the southern margin of the High Atlas is supported by geophysical results, heat flow data show a steeply dipping high conductivity zone (Rimi, 1999) and seismic tomography and shear-wave splitting analyses (e.g., Palomeras *et al*.,

2014; Miller *et al*., 2014) indicate that a significant (up to 26 km offset; Miller *et al*., 2014) and steep step in the lithospheric thickness occurs across the SAF. These data are interpreted to correspond to a reactivated and inverted Mesozoic normal fault that is accommodating the uplift related to the convective removal of the lithospheric root to the Atlas during the Quaternary (Miller *et al*., 2014). Therefore, our analyses suggest that knickpoint generation and landscape rejuvenation recorded in the fluvial systems is responding to reactivation of these crustal-scale reverse faults and not to activity on low-angle faults at the edge of the thrust front, supporting the results from geophysical imaging. Although, we cannot differentiate between models showing the location of this high-angle structure at the thrust front or further into the hinterland.

CONCLUSIONS

We used stream profiles to analyse patterns in channel steepness and incision for rivers draining southwards from the central High Atlas across the South Atlas Fault along the northern margin of the Ouarzazate Basin. As the timing and mechanisms for recent uplift in the High Atlas Mountains of Morocco are still under debate (e.g., Gomez et al., 2000; El Harfi et al., 2001; 2006; Barbero et al., 2007) these analyses have derived new information on the Plio-Quaternary landscape evolution that can be linked to tectonics. The rivers, forming the principle trunk drainage system of the Dades-Draa catchment, are characterised by the presence of one or more knickpoints on the river long profiles. Knickpoint retreat distance is shown to scale with drainage area, which is characteristic of a single knickpoint formation event. Furthermore, the normalised steepness index (k_{sn}) increases below knickpoints (slope-break type) indicative of higher uplift rates downstream than above and the magnitude of calculated incision correlates with other geological estimates of uplift (e.g., Teixell et al., 2003; 2005; Balestrieri et al., 2009). We also rule out mechanisms of knickpoint formation due to lithological contrasts and river capture. Thereby we conclude that the knickpoints record a transient erosional response to an increase in rock uplift upon a fault, probably with a planar geometry, during the Plio-Quaternary. Comparison to previous studies suggests that this structure may represent an inverted normal fault that initially formed during Jurassic rifting and subsequently reactivated due to regional compression and removal of the lithospheric root of the High Atlas Mountains. Although, the rates and timings of uplift and incision need more accurate constraints to further clarify relationships, our analysis clearly demonstrates that in regions lacking quantitative data, stream profile analysis can be a powerful tool for understanding the underlying geodynamics of a collisional mountain belt system.

ACKNOWLEDGMENTS

We thank National Geographic (Grant no - 8609-09) for funding this project, and for the editor - Laurent Jolivet, Loreto Anton and anonymous reviewers for their constructive comments that have greatly improved this contribution

REFERENCES

Antón, L., Rodés, A., De Vicente, G., Pallàs, R., Garcia-Castellanos, D., Stuart, F. M., Braucher, R., & Bourlès, D., 2012. Quantification of fluvial incision in the Duero Basin (NW Iberia) from

longitudinal profile analysis and terrestrial cosmogenic nuclide concentrations. Geomorphology, 165, 50-61.

Antón, L., De Vicente, G., Muñoz-Martín, A., & Stokes, M., 2014. Using river long profiles and geomorphic indices to evaluate the geomorphological signature of continental scale drainage capture, Duero basin (NW Iberia). Geomorphology, 206, 250-261. DOI: 10.1016/j.geomorph.2013.09.028

Arboleya, M.L., Teixell, A. and Julivert, M., 2004, A structural transect through the high and middle Atlas of Morocco: Journal of African Earth Sciences, v. 39, p. 319–327.

Arboleya, M-L., Babault, J., Owen, L.A., Teixell, A. and Finkel, R.C., 2008, Timing and nature of Quaternary fluvial incision in the Ouarzazate foreland basin, Morocco: Journal of the Geological Society [London], v. 165, p. 1059-1073.

Babault, J.A., Teixell, A., Arboleya M.L., Charroud, M., 2008. A Late Cenozoic age for the long-wavelength surface uplift of the Atlas Mountains of Morocco. Terra Nova, 20, 102-107.

Babault, J., Van Den Driessche, J., and Teixell, A., 2012. Longitudinal to transverse drainage network evolution in the High Atlas (Morocco): The role of tectonics. Tectonics, 31(4).

Balestrieri, M.L., Moratti, G., Bigazzi, G., and Algouti, A., 2009. Neogene exhumation of the Marrakech High Atlas (Morocco) recorded by apatite fission-track analysis: Terra Nova, v. 21, p. 75–82.

Barbero, L., Teixell, A., Arboleya, M. L., Río, P. D., Reiners, P. W., and Bougadir, B. 2007. Jurassic-to-present thermal history of the central High Atlas (Morocco) assessed by low-temperature thermochronology. Terra Nova, 19(1), 58-64.

Beauchamp, W., Allmendinger, R. W., Barazangi, M., Demnati, A., El Alji, M., and Dahmani, M. 1999. Inversion tectonics and the evolution of the High Atlas Mountains, Morocco, based on a geological-geophysical transect. Tectonics, 18(2), 163-184.

Berlin, M.M., and Anderson, R.S., 2007. Modeling of knickpoint retreat on the Roan Plateau, western Colorado. Journal of Geophysical Research, 112: F03S06. Doi:10.1029/2006JF000553

Bishop, P., Hoey, T. B., Jansen, J. D., and Artza, I. L., 2005. Knickpoint recession rate and catchment area: The case of uplifted rivers in eastern Scotland. Earth Surface Processes and Landforms, 30(6), 767-778.

Boulton, S. J. and Whittaker, A.C., 2009, Quantifying the slip rates, spatial distribution and evolution of active normal faults from geomorphic analysis: Field examples from an oblique-extensional graben, southern Turkey: Geomorphology, v. 104, p. 299-316.

Brocklehurst, S.H., 2010, Tectonics and geomorphology: Progress in Physical Geography, v. 34, p. 357-383.

Burbank, D.W., and Anderson, R.S., 2001. Tectonic Geomorphology. Blackwell, Oxford, UK.

Cappy, S., 2006. Hydrological characterization of the Upper Draa Catchment: Morocco. Unpublished Ph.D Dissertation, Rheinischen Friedich-Wilhelm-Universität Bonn, Germany.

Castillo, M., Bishop, P., and Jansen, J. D. 2013. Knickpoint retreat and transient bedrock channel morphology triggered by base-level fall in small bedrock river catchments: The case of the Isle of Jura, Scotland. Geomorphology, 180-181, 1-9.

Clark, M.K., Maheo, G., Saleeby, J., Farley, K.A., 2005. The non-equilibrium landscape of the southern Sierra Nevade, California. GSA Today, 15, 4-10.

Cook, K. L., Whipple, K.X., Heimsath, A.M., Hanks, T. C., 2009. Rapid incision of the Colorado River in Geln Canyon – insights from channel profiles, local incision rates, and modelling of lithologic controls. Earth Surface Processes and Landforms, 34, 994 – 1010.

Crosby, B. T., and Whipple, K. X., 2006, Knickpoint initiation and distribution within fluvial networks, 236 waterfalls in the Waipaoa River, North Island, New Zealand: Geomorphology, v. 82, p. 16-38.

Crosby, B. T., Whipple, K. X., Gasparini, N. M., & Wobus, C. W., 2007. Formation of fluvial hanging valleys: Theory and simulation. Journal of Geophysical Research: Earth Surface, 112(F3).

Cyr, A.J., Granger, D.E., Olivetti, V., Molin, P., 2010. Quantifying rock uplift rates using channel steepness and cosmogenic nuclide-determined erosion rates: examples from northern and southern Italy. Lithosphere, 2, 188-198.

D'Arcy, M., & Whittaker, A. C., 2014. Geomorphic constraints on landscape sensitivity to climate in tectonically active areas. Geomorphology, 204, 366-381.

DiBiase, R.A., Whipple, K.X., Heimsath, A.M., Ouimet, W.B., 2009. Landscape form and millennial erosion rates in the San Gabriel Mountains, California. Earth and Planetary Science Letters, 289, 134-144.

Duvall, A., Kirby, E., & Burbank, D. 2004. Tectonic and lithologic controls on bedrock channel profiles and processes in coastal California. Journal of Geophysical Research: Earth Surface (2003–2012), 109(F3).

El Harfi, A., Lang, J., Salomon, J., and Chellai, E. H., 2001, Cenozoic sedimentary dynamics of the Ouarzazate foreland basin (central High Atlas Mountains, Morocco): International Journal of Earth Science, v. 90, p. 393-411.

El Harfi, A., Guiraud, M., and Lang, J., 2006. Deep-rooted ‘‘thick skinned’’ model for the High Atlas Mountains (Morocco). Implications for the structural inheritance of the southern Tethys passive margin: Journal of Structural Geology, v. 28, p. 1958-1976.

Frizon de Lamotte, D., B. Saint Bezar, R. Bracene, and E. Mercier, 2000. The two main steps of the Atlas building and geodynamics of the western Mediterranean, Tectonics, 19, 740 – 761,.

Frizon De Lamotte, D.., Leturmy, P., Missenard, Y., Khomsi, S., Ruiz, G., Saddiqi, O., Guillocheau, F. and Michard, A. 2009. Mesozoic and Cenozoic vertical movements in the Atlas system (Algeria, Morocco, Tunisia): an overview. Tectonophysics, 475(1), 9-28.

Garbrect, J., Martz, L.W., 1997. The assignment of drainage direction over flat surfaces in raster digital elevation models. Journal of Hydrology, 193, 204-213.

Gomez, F., Beauchamp, W., and Barazangi, M., 2000, Role of the Atlas Mountains (northwest Africa) within the African-Eurasian plate-boundary zone: Geology, v. 28, p. 775–778.

Goldrick, G., and Bishop, P., 2007. Regional analysis of bedrock stream long profiles: evaluation of Hack's SL form, and formulation and assessment of an alternative (the DS form). Earth Surface Processes and Landforms, 32(5), 649-671.

Görler, K., Helmdach, F.F., Gaemers, P., Heissig, K., Hinsch, W., Mädler, K., Shwarzhans, W., and Zucht, M., 1988, The uplift of the central High Atlas as deduced from Neogene continental

sediments of the Ouarzazate province, Morocco: Lecture Notes in Earth Sciences, v. 15, p. 363–404.

Harkins, N., Kirby, E., Heimsath, A., Robinson, R., Reiser, U., 2007. Transient fluvial incision in the headwaters of the Yellow River, northeastern Tibet, China. Journal of Geophysical Research – Earth Surface, 112: F03S04.

Hasbargen, L.E., and Paola, C., 2000, Landscape instability in an experimental drainage basin: Geology, v. 28, p. 1067–1070.

Hoke, G.D., Isacks, B.L., Jordan, T.E., Blanco, N,. Tomlinson, A.J., Ramezani, J., 2007. Geomorphic evidence for post-10Ma uplift of the western flank of the central Andes 18º30' - 22ºS. Tectonics, 26, TC5021.

Hughes, P.D. Gibbard, P.L. and Woodward J.C., 2004, Quaternary glaciation in the Atlas Mountains of North Africa: Developments in Quaternary Science, v. 2, Part 3, p. 255-260.

Jansen, J. D., Fabel, D., Bishop, P., Xu, S., Schnabel, C., and Codilean, A. T. 2011. Does decreasing paraglacial sediment supply slow knickpoint retreat?. Geology, 39(6), 543-546.

Kirby, E., Ouimet, W., 2011. Tectonic geomorphology along the eastern margin of the Tibet: insights into the pattern and processes of active deformation adjacent to the Sichuan Basin. In: Gloguen, R., Ratschbacher, L. (eds). Growth and collapse of the Tibetan Plateau. Geological Society, London Special Publications, 353, 165-188.

Kirby, E., and Whipple, K.X., 2001, Quantifying differential rock-uplift rates via stream profile analysis: Geology, v. 29, p. 415-418.

Kirby, E., and Whipple, K.X., 2012. Expression of active tectonics in erosional landscapes. Journal of Structural Geology, 44, 54-75.

Kirby, E., Whipple, K.X., Tang, W., and Chen, Z., 2003, Distribution of active rock uplift along the eastern margin of the Tibetan Plateau: Inferences from bedrock river profiles: Journal of Geophysical Research, v.108, 2217, doi:10.1029/2001JB000861.

Kirby, E., Johnson, C., Furlong, K., and Heimsath, A., 2007, Transient channel incision along Bolinas Ridge, California: evidence for differential rock uplift adjacent to the San Andreas Fault: Journal of Geophysical Research, v. 112, F03S07, doi:10.1029/2006JF000559.

Medina, F., Cherkaoui, T-E., 1991. Focal mechanisms of the Atlas earthquakes, and tectonic implications. Geologische Rundschau, 80, 639 – 648.

Miller, M. S., Becker, T. W., 2014. Reactivated lithospheric-scale discontinuities localize dynamic uplift of the Moroccan Atlas Mountains. Geology, 42(1), 35-38.

Miller, S.R., Baldwin, S.L., Fitzgerald, P.G., 2012. Transient fluvial incision and active surface uplift in the Woodlark Rift of eastern Papua New Guinea. Lithosphere, 4, 131-149. Doi:10.1130/L135.1

Missenard, Y., Zeyen, H., Frizon de Lamotte, D., Leturmy, P., Petit, C., Sebrier, M., Saddiqi, O., 2006. Crustal versus asthenospheric origin of relief of the Atlas Mountains of Morocco. Journal of Geophysical research, 111, B03401 doi:10.1029/2005JB003708.

Morel, J. L., and Meghraoui, M., 1996, The Goringe-Alboran-Tell (GALTEL) tectonic zone, a transpression system along the Africa-Eurasia plate boundary: Geology, v. 24, p. 755-758.

Neimann, J.D., Gasparini, N.M., Tucker, G.E., and Bras, R.L., 2001, A quantitative evaluation of Playfair's law and its use in testing long-term stream erosion models: Earth Surface Process and Landforms, v. 26, p. 1317-1332.

Onana, P. N. E., Zouhri, L., Chaabane, A., El Mouraouah, A., Brahim, A. I., 2011. Recent seismicity of Central High Atlas and Ouarzazate basin (Morocco). Bulletin of Engineering Geology and the Environment, 70, 633-641.

Ouimet, W. B., Whipple, K. X., and Granger, D. E. 2009. Beyond threshold hillslopes: Channel adjustment to base-level fall in tectonically active mountain ranges. Geology, 37(7), 579-582.

Palomeras, I., Thurner, S., Levander, A., Liu, K., Villasenor, A., Carbonell, R., and Harnafi, M. 2014. Finite-frequency Rayleigh wave tomography of the western Mediterranean: Mapping its lithospheric structure. Geochemistry, Geophysics, Geosystems. DOI: 10.1002/2013GC004861

Pastor, A., Teixell, A., and Arboleya, M.L., 2012a. Rates of Quaternary deformation in the Ouarzazate Basin (Southern Atlas Front, Morocco). Annals of Geophysics, 55 (5) 1003 – 1016 doi:10.4401/ag-4940

Pastor, A., Babulat, J., Teixell, A., Arboleya, M.L., 2012b. Intrinsic stream-capture control of stepped fan pediments in the High Atlas piedmont of Ouarzazate (Morocco). Geomorphology, 173-174, 88-103.

Phillips J.D. and Lutz, J.D., 2008, Profile convexities in bedrock and alluvial streams: Geomorphology, v. 102, p. 554–566.

Ramdani, F. 1998. Geodynamic implications of intermediate-depth earthquakes and volcanism in the intraplate Atlas mountains (Morocco). Physics of the Earth and Planetary Interiors, 108(3), 245-260.

Regalla, C., Kirby, E., Fisher, D., and Bierman, P., 2013. Active forearc shortening in Tohoku, Japan: Constraints on fault geometry from erosion rates and fluvial longitudinal profiles. Geomorphology, 195, 84-98.

Rimi, A., 1999. Mantle heat flow and geotherms for the main geologic domains in Morocco. International Journal of Earth Sciences, 88(3), 458-466.

Saadi, M., Hilali, E.A., Boudda, A., 1978. Ouarzazate 1:500000 Geological Map, Ministry of Energy and Mines, Geology Directorate, Kingdom of Morocco.

Safran, E.B., Bierman, P.R., Aalton, R., Dunne, T., Whipple, K.X., Cafee, M., 2005. Erosion rates driven by channel network incision in the Bolivian Andes. Earth Surface Processes and Landforms, 30, 1007 – 1024.

Schildgen, T. F., Cosentino, D., Bookhagen, B., Niedermann, S., Yıldırım, C., Echtler, H., Whittmann, and Strecker, M. R., 2012. Multi-phased uplift of the southern margin of the Central Anatolian plateau, Turkey: A record of tectonic and upper mantle processes. Earth and Planetary Science Letters, 317, 85-95.

Schoenbohm, L.M., Whipple, K.X., Burchfield, B.C., Chen, L., 2004. Geomorphic constrains on surface uplift, exhumation and plateau growth in the Red River region, Yunnan Province, China. Geological Society of America Bulletin, 116, 895-909.

Schumm, S.A., 2005. River Variability and Complexity. Cambridge University Press, New York.

Seber, D., Barazangi, M., Tadili, B.A., Ramdami, M., Ibenbrahim, A., Ben Sari, D., 1996. Three-dimensional upper mantle structure beneath intraplate Atlas and interplate Rif Mountains of Morocco. Journal of Geophysical Research, 101, 3125-3138.

Sebrier, M., Siame, L., Zouine, E. M., Winter, T., Missenard, Y. and Leturmy, P., 2006, Active tectonics in the Moroccan High Atlas: Compte Rendus Geoscience, v. 338, p. 65-79.

Snyder, N.P., Whipple, K.X., Tucker, G.E. and Merrits, D.J., 2000, Landscape response to tectonic forcing: digital elevation model analysis of stream profiles in the Mendocino triple junction region, Northern California: Geological Society of America Bulletin, v. 112, p. 1250-1263.

Stäblein, G., 1988. Geomorphological aspects of the Quaternary evolution of the Ouarzazate Basin, Southern Morocco: Lecture Notes in Earth Sciences, v. 15, p. 433–443.

Stokes, M., Mather, A. E., & Harvey, A. M., 2002. Quantification of river-capture-induced base-level changes and landscape development, Sorbas Basin, SE Spain. Geological Society, London, Special Publications, 191(1), 23-35.

Stokes, M., Mather, A.E., Belfoul, A. and Farik, F., 2008, Active and passive tectonic controls for transverse drainage and river gorge development in a collisional mountain belt (Dades Gorges, High Atlas Mountains, Morocco): Geomorphology, v. 102, p. 2-20.

Teson, E. and Teixell, A., 2008, Sequence of thrusting and syntectonic sedimentation in the eastern sub-Atlas thrust belt (Dades and Mgoun valleys, Morocco): International Journal of Earth Sciences, v. 97, p. 103–113.

Teixell, A., Arboleya, M.-L., and Julivert, M., 2003. Tectonic shortening and topography in the central High Atlas (Morocco): Tectonics, v. 22, p. 1–13.

Teixell, A., Ayarza, P., Zeyen, H., Fernandez, M., Arboleya, M.L., 2005. Effects of mantle upwelling in a compressional setting: the Atlas Mountains of Morocco. Terra Nova, 17, 456-461.

Teson, E., Puyoe, E.L., Teixell, A., Barnolas, A., Agusti, J., Furio, M., 2010. Magnetostratigraphy of the Ouarzazte Basin: Implications for the timing of deformation and mountain building in the High Atlas Mountains of Morocco. Geodinamica Acta, 23, 151-165.

Tucker, G. E., 2009, Natural experiments in landscape evolution: Earth Surface Processes and Landforms, v. 34, p. 1450-1460

Tucker, G. E., and Whipple, K. X., 2002, Topographic outcomes predicted by stream erosion models: sensitivity analysis and inter-model comparison. v. 107, B9, p. 2179, doi:10.1029/2001JB000162.

Tucker, G. E., and Hancock, G.R., 2010, Modelling landscape evolution: Earth Surface Processes Landforms, v. 35, p. 28–50.

USGS 2006, Shuttle Radar Topography Mission, 3 Arc Second scene SRTM_p201r038, Filled Finished-B, Global Land Cover Facility, University of Maryland, College Park, Maryland, February 2000.

USGS, 2010. National Earthquake Information Centre. http://earthquake.usgs.gov/regional/neic/ accessed 24 August 2011.

Walsh, L.S., Martin, A.J., Ojha, T.P., Fedenczuk, T., 2012. Correlations of fluvial knickpoints with landslide dams, lithologic contacts, and faults in the southwestern Annapurna Range, central

Nepalese Himalaya. Journal of Geophysical Research, 117: F01012. Doi:10.1029/2011JF001984.

Whipple, K.X., 2004. Bedrock rivers and the geomorphology of active orogens. Annual review of Earth and Planetary Sciences, 32, 151-185.

Whipple, K.X., and Tucker, G.E., 1999, Dynamics of the stream power incision model: implications for the height limits of mountain ranges, landscape response timescales and research needs. Journal Geophysical Research, v. 104, p. 17661-17674.

Whipple, K.X., and Tucker, G.E., 2002, Implications of sediment-flux dependent river incision models for landscape evolution: Journal Geophysical Research, v. 107(B2), doi: 10.1029/2000JB044

Whittaker, A. C., and Boulton, S. J., 2012. Tectonic and climatic controls on knickpoint retreat rates and landscape response times, Journal of Geophysical Research-Earth Surface, 117:F02024, doi:10.1029/2011JF002157

Whittaker, A.C., Cowie, P.A., Attal, M., Tucker, G.E., and Roberts, G., 2007. Contrasting transient and steady-state rivers crossing active normal faults: new field observations from the Central Appenines, Italy: Basin Research, v. 19, p. 529-556.

Whittaker, A.C., Attal, M., Cowie, P.A., Tucker, G.E., and Roberts, G., 2008. Decoding temporal and spatial patterns of fault uplift using transient river long profiles: Geomorphology, v. 100, p. 506-526.

Willemin, J. H., 2000. Hack's Law: Sinuosity, convexity, elongation, *Water Resources Research*, 36(11), 3365–3374, doi:10.1029/2000WR900229.

Wobus, C.W., Hodges, K.V., and Whipple, K.X., 2003. Has focussed denudation sustained active thrusting at the Himalayan topographic front? Geology, v. 31, p.861-864.

Wobus, C.W., Whipple, K.X., Kirby E., Snyder, N., Johnson, J., Spyropolou, K., Crosby, B., and Sheehan, D., 2006, Tectonics from topography: procedures, promise, pitfalls. In: Willett, S., Hovius, N., Brandon, M., Fisher, D., (Eds.), Tectonics, Climate and Landscape Evolution. GSA Special Paper 3

Wohl, E.E., Merritt, D.M., 2001. Bedrock channel morphology. Geological Society of America Bulletin 113:1205-121298, 55-74.

Channel number	River length (km)	Drainage area (km^2)	Distance along strike	Above knickpoint							Below knickpoint							
				Θ	±	K_s	±	K_{sn} = 0.45	±	K_{sn} = 0.60	Θ	±	K_s	±	K_{sn} = 0.45	±	K_{sn} = 0.60	±
Rivers with knickpoints																		
1	123.5	1614.5	0.0	0.26	0.02	2.9	0.9	36.6	2.8	241.6	23.4							
2	88.8	1614.5	0.0	0.44	0.01	73.7	14.0	85.9	1.5	701.7	22.5							
4	104.4	1325.6	20.0	0.61	0.04	797.6	445.9	73.9	2.7	685.3	16.7	0.89	0.14	207670.0	499214.6	92.9	6.0	1346.3	78.5
5	95.8	1325.6	20.0	0.54	0.05	523.7	438.3	131.6	6.6	571.5	38.8	0.04	0.11	0.2	0.4	152.9	6.2	1675.8	85.2
7	77.1	1325.6	20.0	0.72	0.03	10883.2	6285.3	184.9	7.2	1768.4	42.0	0.62	0.07	6223.0	7164.5	331.5	3.7	1789.1	81.0
8	56.0	335.9	44.0	0.63	0.03	984.3	555.6	43.9	2.9	577.4	12.2	0.68	0.64	7430.8	91111.0	89.9	9.8	1623.1	175.9
10	56.5	473.4	54.0	0.12	0.03	1.2	0.5	124.0	8.2	889.9	81.9	0.55	0.10	2599.9	4308.4	509.5	11.3	2591.9	131.0
12	47.3	473.4	54.0	0.50	0.04	87.3	39.8	48.5	1.5	309.6	11.0	0.28	0.02	2.7	1.1	49.8	3.0	558.0	49.8
13	55.1	196.7	62.0	0.47	0.02	187.7	57.8	137.8	3.3	1078.8	37.1	0.80	0.14	96952.9	231852.0	211.8	17.1	3042.3	227.5
14	50.0	314.5	73.4	0.48	0.03	115.5	53.0	73.6	1.8	536.7	19.0	0.50	0.05	530.7	419.4	217.4	8.4	2533.2	100.7
16	45.3	493.5	73.4	0.57	0.08	530.2	602.7	111.0	6.9	842.7	46.0	1.16	0.35	20248765.0	172669.2	146.0	10.8	1806.7	127.3
19	60.3	400.4	84.0	0.63	0.06	919.3	740.4	75.6	3.2	597.4	19.0	0.88	0.09	212735.3	340893.0	127.9	7.2	1718.6	84.1
18	60.3	400.4	90.7	0.98	0.09	135261.0	177091.0	79.8	5.6	661.2	34.2	1.06	0.12	4983407.0	9838829.0	130.3	8.2	1753.2	96.8
20	64.3	400.4	90.7	0.59	0.03	570.9	237.6	79.8	1.8	664.5	10.7	0.41	0.32	40.7	236.2	93.2	12.7	1463.9	203.3
23	49.9	343.0	106.8	0.59	0.01	949.1	194.1	121.8	2.5	1096.6	12.0	1.06	0.11	4740611.1	9037423.0	70.4	4.8	1118.5	62.6
24	63.1	773.5	117.0	0.41	0.02	42.2	11.4	80.9	3.6	488.4	18.3	0.84	0.10	177013.0	337571.0	117.6	7.1	2001.7	105.8
25*	65.7	773.5	120.7	1.15	0.09	9.2×10^7	1×10^7	127.7	8.3	1453.7	76.3	0.42	0.07	49.3	69.4	74.4	3.4	1348.1	67.8
				0.91	0.0	40767.7	19185.8	78.7	4.6	601.5	23.5								
26*	60.1	773.5	120.7	0.53	0.03	243.3	102.6	69.8	1.8	758.8	18.8	0.64	0.09	3067.4	5292.5	86.6	3.4	1627.8	57.5
				0.76	0.0	2601.7	1315.8	59.2	3.7	364.7	12.9								
27*	55.4	773.5	120.7	0.87	0.08	39530.3	48947.1	39.4	2.9	476.8	31.9	0.41	0.05	33.3	29.7	76.3	3.1	1233.8	96.6
				0.58	0.0	186.2	99.7	37.7	1.6	254.7	9.8								
28	45.7	486.5	131.1	0.35	0.03	11.1	3.8	39.2	1.3	272.8	17.3	0.30	0.01	5.2	1.1	42.4	2.0	1193.9	49.3
29	65.1	486.1	134.3	0.69	0.05	3913.2	2780.2	128.5	3.7	1097.0	21.6	0.56	0.04	533.9	369.6	70.3	2.3	1031.9	30.8
Rivers without knickpoints																			
3	56.4	1614.5	0.0									0.25	0.04	2.1	1.4	63.7	2.8	760.1	44.1
6	70.3	1325.6	20.0									0.47	0.01	196.7	26.9	154.6	2.2	1211.2	31.2
9	25.5	335.9	48.0									0.97	0.06	38327.3	28303.0	47.5	3.9	342.1	14.0
11	60.6	473.4	54.0									0.36	0.01	25.9	4.0	84.8	2.0	562.6	21.7

Table 1. River data for the 32 studied rivers; distance along strike is from east to west; Θ = concavity; Ks = steepness index; Ksn = normalised steepness index with reference concavity (either 0.45 or 0.6) stated. * Denotes rivers with second (higher) knickpoint – second line denotes parameters for river channel above this second knickpoint.

			Knickzone (k1)				Knickzone (k2)			
Channel	River length (km)	Drainage area (km^2)	Elevation (m)	Incision* (m)	±	D_{kp} (km)	Elevation (m)	Incision* (m)	±	D_{kp} (km)
1	123.5	1614.5	1905.0	220.0	145.0	56.0				
2	88.8	1614.5	1905.0	220.0	145.0	27.0				
4	104.4	1325.6	2390.0	480.0	7.0	27.0	2872.0	1006.0	95.0	7.1
5	95.8	1325.6	2810.4	889.0	30.0	2.8				
7	77.1	1325.6	2687.0	340.0	130.0	5.9				
8	56.0	335.9	1780.0			17.5				
10	56.5	473.4	2686.2	660.0	214.0	5.1				
12	47.3	473.4	1852.2	107.0	27.0	5.7				
13	55.1	196.7	2293.0	440.0	18.0	6.7				
14	50.0	314.5	2737.0	860.0	14.0	2.9				
16	45.3	493.5	2284.0	531.0	23.0	2.8				
19	60.3	400.4	2232.8	570.0	16.0	5.2				
18	60.3	400.4	2254.0	590.0	20.0	5.2				
20	64.3	400.4	1739.0	131.0	35.0	13.0				
23	49.9	343.0	1523.9	160.0	38.0	15.0				
24	63.1	773.5	2072.6	495.0	10.0	8.7				
25	65.7	773.5	1645.3	140.0	30.0	22.0	2105.2	598.0	27.0	4.8
26	60.1	773.5	1645.3	200.0	7.0	19.0	2086.0	384.0	16.0	2.3
27	55.4	773.5	1712.0	160.0	20.0	20.0				
28	45.7	486.5	1995.0	410.0	16.0	4.0				
29	65.1	486.1	1950.0	80.0	32.0	4.0	2671.0	595.0	30.0	2.2

Table 2. Characteristics of knickpoints in the study area. *Incision is calculated by projecting the long profile above the knickpoint downstream. Dkp = distance downstream from headwaters to knickpoint.